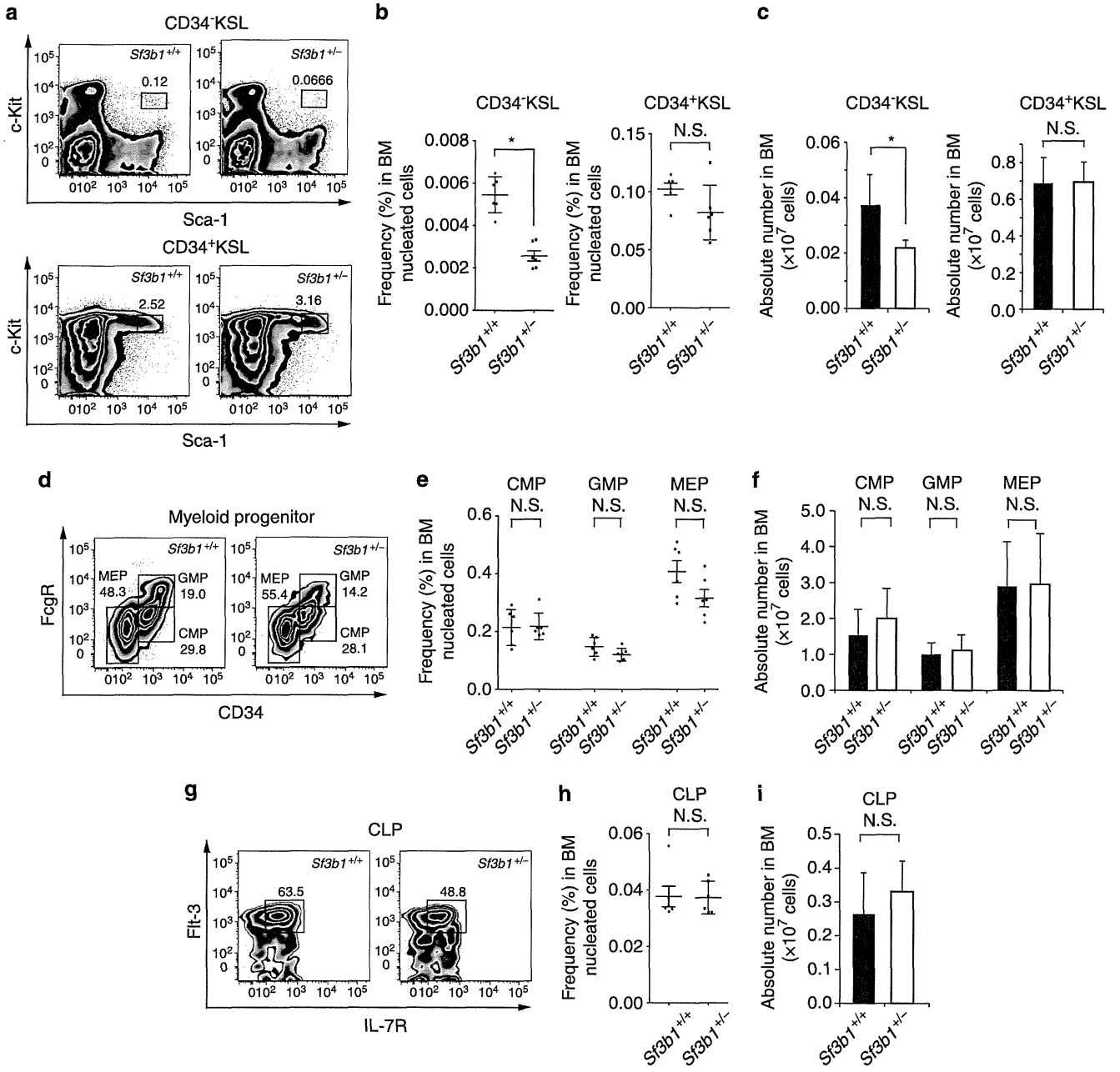

Figure 2. HSC population decreases in *Sf3b1*$^{+/-}$ mice. (**a**) Representative flow cytometric plot of HSCs (CD34$^-$KSL cells) and hematopoietic progenitor cells (HPCs; CD34$^+$KSL cells) from *Sf3b1*$^{+/+}$ and *Sf3b1*$^{+/-}$ mice. (**b**) Frequency of CD34$^-$KSL cells and CD34$^+$KSL cells in *Sf3b1*$^{+/+}$ and *Sf3b1*$^{+/-}$ mice BM. (**c**) Absolute number of CD34$^-$KSL cells and CD34$^+$KSL cells in *Sf3b1*$^{+/+}$ and *Sf3b1*$^{+/-}$ mice BM. (**d**) Representative flow cytometric plot of common myeloid progenitors (CMPs), granulocyte–monocyte progenitors (GMPs) and megakaryocyte–erythroid progenitors (MEPs) in *Sf3b1*$^{+/+}$ and *Sf3b1*$^{+/-}$ mice BM cells. CMPs are defined as Lin$^-$cKIT$^+$Sca1$^-$CD34$^{+/low}$FcgR^{int}, GMPs as Lin$^-$cKIT$^+$Sca1$^-$CD34$^+$FcgR$^+$ and MEPs as Lin$^-$cKIT$^+$Sca1$^-$CD34$^-$FcgR$^-$. (**e**) Frequency of CMPs, GMPs and MEPs in *Sf3b1*$^{+/+}$ and *Sf3b1*$^{+/-}$ mice BM. (**f**) Absolute number of CMPs, GMPs and MEPs in *Sf3b1*$^{+/+}$ and *Sf3b1*$^{+/-}$ mice BM. (**g**) Representative flow cytometric plot of common lymphoid progenitors (CLPs) in *Sf3b1*$^{+/+}$ and *Sf3b1*$^{+/-}$ mice BM cells. CLPs are defined as Lin$^-$ ckit^{low} Sca1^{low}IL7R$^+$Flt3$^+$. (**h**) Frequency of CLPs in *Sf3b1*$^{+/+}$ and *Sf3b1*$^{+/-}$ mice BM. (**i**) Absolute number of CLPs in *Sf3b1*$^{+/+}$ and *Sf3b1*$^{+/-}$ mice BM. Data are the mean ± s.d.; $n = 6$ per genotype. *$P < 0.05$. NS, not significant.

wild-type mice were detected (Supplementary Figure 3a and Supplementary Tables 4 and 5). Expression of *Sf3b1* in HSCs from *Sf3b1*$^{+/-}$ mice was reduced by ~45% compared with that in *Sf3b1*$^{+/+}$ HSCs, and this was confirmed by quantitative reverse transcriptase-PCR (Supplementary Figure 3b). Next, we performed the pathway analysis for differential expressed genes using GSEA, but GSEA identified no significant biological pathways, which explained the functional impairments in HSCs of *Sf3b1*$^{+/-}$ mice.

DISCUSSION

The *SF3B1* mutation is one of the most frequent genetic alterations in myelodysplasia and is also found in some chronic lymphocytic leukemia cases. Hence, the physiological role of *SF3B1* in the regulation of normal hematopoiesis provides an important clue to understand the role of *SF3B1* mutations in the pathogenesis of hematopoietic malignancies having the *SF3B1* mutation. Here, we showed

© 2014 Macmillan Publishers Limited

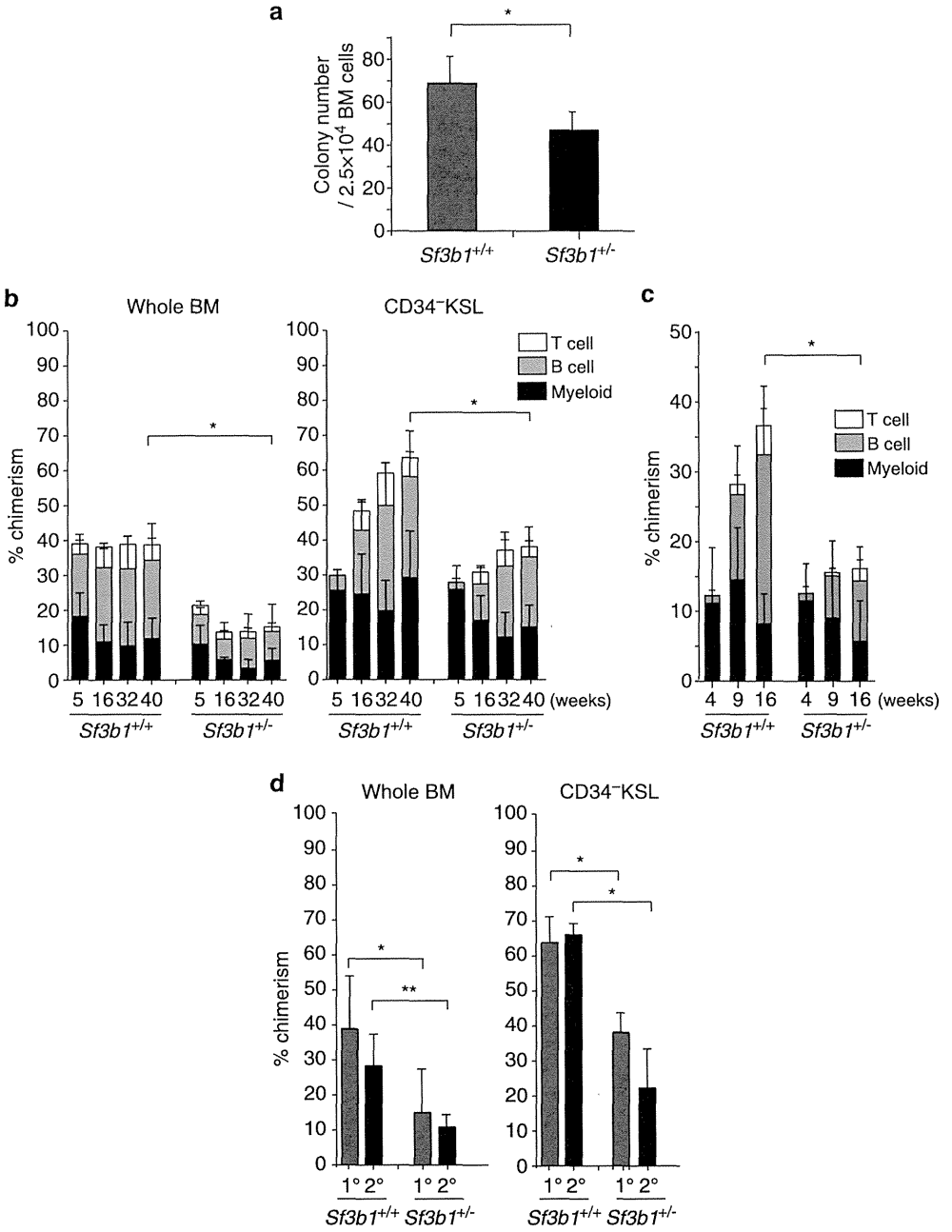

Figure 3. Reduced HSC numbers and impaired HSC function in *Sf3b1*$^{+/-}$ mice. (**a**) Total number of colony-forming units generated from whole BM cells. The number of colonies was counted after 14 days of culture. Data are the mean ± s.d.; $n=4$ per genotype; *$P<0.05$. (**b**) Competitive transplantation using whole BM or HSCs; the vertical axis represents the average peripheral blood (PB) chimerism of donor-derived CD45.2$^+$ cells. Data are the mean ± s.d.; $n=13$ for whole BM transplantation, $n=8$ for HSC transplantation; *$P<0.05$. (**c**) Competitive transplantation using enriched long-term HSCs (CD150$^+$CD34$^-$KSL cells); the vertical axis represents the average PB chimerism of donor-derived CD45.2$^+$ cells. Data are shown as mean ± s.d.; $n=5$, *$P<0.05$. (**d**) Serial transplantation assay; at 40 weeks post primary transplantation, BM cells harvested from the recipient mice were serially transplanted into additional secondary recipient mice. Chimerism of donor-derived CD45.2$^+$ cells in peripheral blood at 40 weeks after primary transplantation (1°) and at 21 weeks after secondary transplantation (2°). Data are the mean ± s.d.; $n=13$ for primary whole BM transplantation, $n=8$ for primary HSC transplantation and $n=5$ for both secondary transplantation per group; *$P<0.05$, **$P<0.01$.

unequivocally that *SF3B1* plays an important role in the regulation of HSCs.

In the present study, *Sf3b1*$^{+/-}$ mice showed a significantly reduced number of HSCs and compromised reconstitution capacity of hematopoiesis, although the underlying molecular mechanism remained elusive. SF3B1 is known as a core component of the mRNA splicing machinery, and therefore a possible mechanism would be altered RNA splicing caused by haploinsufficiency of the genes involved in stem cell regulation. Unfortunately, we failed to identify plausible genes whose splicing was specifically altered in *Sf3b1*$^{+/-}$ mice. The other possibility is that the mechanism is not related to RNA splicing. In fact, *Sf3b1*$^{+/-}$ mice have been reported to show posterior transformation of vertebrae, and this phenomenon was ascribed to deregulation of the expression of *Hox* genes without any accompanying defects in *Hox* gene splicing. The deregulated *Hox* gene expression is

© 2014 Macmillan Publishers Limited

thought to be caused by compromised Polycomb activities because of *Sf3b1* haploinsufficiency.[12] Polycomb group proteins are epigenetic transcriptional repressors with an important role in the regulation of hematopoiesis, and recent studies have shown that mutations in Polycomb group genes occur in hematological neoplasms (including MDS).[25,26] Furthermore, most *Hox* genes are expressed in HSCs and immature progenitors and are downregulated during differentiation and maturation, and the critical role of Hox gene clusters in normal hematopoiesis has been demonstrated repeatedly in many literatures.[27,28] For example, overexpression of *Hoxb4* leads to expansion of HSCs, and *Hoxb4*-deficient mice exhibit a reduced reconstitution capacity similar to that seen in *Sf3b1*$^{+/-}$ mice.[29] Similarly, *Hoxa 9* and *10* are also reported to be functional regulators of HSCs.[30,31] However, in our gene expression data based on RNA sequencing, expression of *Hoxb4* was increased in HSCs from *Sf3b1*$^{+/-}$ mice compared with that from *Sf3b1*$^{+/+}$ mice, and other clustered *Hox* genes, including *Hoxa9* and *10*, were not significantly changed (Supplementary Figure 3b). Thus, the exact mechanism of action that leads to reduced numbers of HSCs and their compromised function remains unclear.

The other important issue to be discussed regarding the phenotype of *Sf3b1*$^{+/-}$ mice is the impact of *Sf3b1* haploinsufficiency upon the formation of ring sideroblasts because the *SF3B1* mutation is closely associated with MDS with increased numbers of ring sideroblasts. Although a previous study reported an increased frequency of ring sideroblasts in *Sf3b1*$^{+/-}$ mice,[21] no increase in ring sideroblasts was demonstrated in the present study, even though both studies analyzed the identical *Sf3b1*$^{+/-}$ mouse strain.[12] However, we considered that the lack of increased numbers of ring sideroblasts, together with the compromised repopulation capacity of *Sf3b1*$^{+/-}$ stem cells, should be rather expected, because most of the *SF3B1* mutations thus far reported in MDS are clustered in the 5th–9th HEAT domains, mainly involving 5 hot spot amino-acid positions (K700 and, to a lesser extent, K666, H662 and E662), and no nonsense or frameshift changes have been reported, suggesting that these *SF3B1* mutations will not lead to simple loss of function but should be associated with some gain of function.[1,2,9] We could not exclude the possibility that an *SF3B1* mutation acts as a dominant negative mutation that leads to more severe functional deficiency than haploinsufficiency, which would be responsible for tumorigenesis. However, our findings suggest that the simple haploinsufficiency of *SF3B1* may not be responsible for the development of the MDS phenotype with increased formation of ring sideroblasts and other clonal disorders. In this regard, *Sf3b1*$^{+/-}$ mice may not be a suitable animal model for MDS, but further functional experiments using a conditional knock-in *Sf3b1* mutant allele is required to understand the molecular mechanisms of *SF3B1* mutations.

CONFLICT OF INTEREST

The authors declare no conflict of interest.

ACKNOWLEDGEMENTS

We thank Y Yamazaki for his excellent technical support on flow cytometric analyses and cell sorting. This work was supported in part of Grants-in-aid for Scientific Research (nos. 24390242 and 23249052) and Grant-in-Aid for Scientific Research on Innovative Areas (no. 4201), MEXT, Japan, and grants from the Princes Takamatsu Cancer Research Fund and the Japan Leukemia Research Fund.

AUTHOR CONTRIBUTIONS

MM, RY, MS, MO and HN performed mouse experiments; MM, AS-O, Y Shiozawa, KY, Y Shiraishi and SM performed bioinformatics analyses of RNA sequencing data; KI and HK generated *Sf3b1* knockout mice; MM, RY, MS and AS-O analyzed the data and generated figures and table; and MM, MS and SO designed the experiments and wrote the manuscript. All authors participated in the discussion and interpretation of data and results.

REFERENCES

1 Yoshida K, Sanada M, Shiraishi Y, Nowak D, Nagata Y, Yamamoto R *et al.* Frequent pathway mutations of splicing machinery in myelodysplasia. *Nature* 2011; **478**: 64–69.
2 Papaemmanuil E, Cazzola M, Boultwood J, Malcovati L, Vyas P, Bowen D *et al.* Somatic SF3B1 mutation in myelodysplasia with ring sideroblasts. *N Engl J Med* 2011; **365**: 1384–1395.
3 Graubert TA, Shen D, Ding L, Okeyo-Owuor T, Lunn CL, Shao J *et al.* Recurrent mutations in the U2AF1 splicing factor in myelodysplastic syndromes. *Nat Genet* 2011; **44**: 53–57.
4 Visconte V, Makishima H, Jankowska A, Szpurka H, Traina F, Jerez A *et al.* SF3B1, a splicing factor is frequently mutated in refractory anemia with ring sideroblasts. *Leukemia* 2012; **26**: 542–545.
5 Wang L, Lawrence MS, Wan Y, Stojanov P, Sougnez C, Stevenson K *et al.* SF3B1 and other novel cancer genes in chronic lymphocytic leukemia. *N Engl J Med* 2011; **365**: 2497–2506.
6 Biankin AV, Waddell N, Kassahn KS, Gingras MC, Muthuswamy LB, Johns AL *et al.* Pancreatic cancer genomes reveal aberrations in axon guidance pathway genes. *Nature* 2012; **491**: 399–405.
7 Stephens PJ, Tarpey PS, Davies H, Van Loo P, Greenman C, Wedge DC *et al.* The landscape of cancer genes and mutational processes in breast cancer. *Nature* 2012; **486**: 400–404.
8 Harbour JW, Roberson ED, Anbunathan H, Onken MD, Worley LA, Bowcock AM. Recurrent mutations at codon 625 of the splicing factor SF3B1 in uveal melanoma. *Nat Genet* 2013; **45**: 133–135.
9 Malcovati L, Papaemmanuil E, Bowen DT, Boultwood J, Della Porta MG, Pascutto C *et al.* Clinical significance of SF3B1 mutations in myelodysplastic syndromes and myelodysplastic/myeloproliferative neoplasms. *Blood* 2011; **118**: 6239–6246.
10 Cazzola M, Rossi M, Malcovati L. Associazione Italiana per la Ricerca sul Cancro Gruppo Italiano Malattie Mieloproliferative. Biologic and clinical significance of somatic mutations of SF3B1 in myeloid and lymphoid neoplasms. *Blood* 2013; **121**: 260–269.
11 Wahl MC, Will CL, Luhrmann R. The spliceosome: design principles of a dynamic RNP machine. *Cell* 2009; **136**: 701–718.
12 Isono K, Mizutani-Koseki Y, Komori T, Schmidt-Zachmann MS, Koseki H. Mammalian polycomb-mediated repression of Hox genes requires the essential spliceosomal protein Sf3b1. *Genes Dev* 2005; **19**: 536–541.
13 Ema H, Morita Y, Yamazaki S, Matsubara A, Seita J, Tadokoro Y *et al.* Adult mouse hematopoietic stem cells: purification and single-cell assays. *Nat Protoc* 2006; **1**: 2979–2987.
14 Yamamoto R, Morita Y, Ooehara J, Hamanaka S, Onodera M, Rudolph KL *et al.* Clonal analysis unveils self-renewing lineage-restricted progenitors generated directly from hematopoietic stem cells. *Cell* 2013; **154**: 1112–1126.
15 Sato Y, Yoshizato T, Shiraishi Y, Maekawa S, Okuno Y, Kamura T *et al.* Integrated molecular analysis of clear-cell renal cell carcinoma. *Nat Genet* 2013; **45**: 860–867.
16 Langmead B, Trapnell C, Pop M, Salzberg SL. Ultrafast and memory-efficient alignment of short DNA sequences to the human genome. *Genome Biol* 2009; **10**: R25.
17 Kent WJ. BLAT—the BLAST-like alignment tool. *Genome Res* 2002; **12**: 656–664.
18 Mortazavi A, Williams BA, McCue K, Schaeffer L, Wold B. Mapping and quantifying mammalian transcriptomes by RNA-Seq. *Nat Methods* 2008; **5**: 621–628.
19 Quinlan AR, Hall IM. BEDTools: a flexible suite of utilities for comparing genomic features. *Bioinformatics* 2010; **26**: 841–842.
20 Subramanian A, Tamayo P, Mootha VK, Mukherjee S, Ebert BL, Gillette MA *et al.* Gene set enrichment analysis: a knowledge-based approach for interpreting genome-wide expression profiles. *Proc Natl Acad Sci USA* 2005; **102**: 15545–15550.
21 Visconte V, Rogers HJ, Singh J, Barnard J, Bupathi M, Traina F *et al.* SF3B1 haploinsufficiency leads to formation of ring sideroblasts in myelodysplastic syndromes. *Blood* 2012; **120**: 3173–3186.
22 Osawa M, Hanada K, Hamada H, Nakauchi H. Long-term lymphohematopoietic reconstitution by a single CD34-low/negative hematopoietic stem cell. *Science* 1996; **273**: 242–245.
23 Kiel MJ, Yilmaz OH, Iwashita T, Yilmaz OH, Terhorst C, Morrison SJ. SLAM family receptors distinguish hematopoietic stem and progenitor cells and reveal endothelial niches for stem cells. *Cell* 2005; **121**: 1109–1121.
24 Morita Y, Ema H, Nakauchi H. Heterogeneity and hierarchy within the most primitive hematopoietic stem cell compartment. *J Exp Med* 2010; **207**: 1173–1182.

© 2014 Macmillan Publishers Limited

25 Radulovic V, de Haan G, Klauke K. Polycomb-group proteins in hematopoietic stem cell regulation and hematopoietic neoplasms. *Leukemia* 2013; **27**: 523–533.
26 Shih AH, Abdel-Wahab O, Patel JP, Levine RL. The role of mutations in epigenetic regulators in myeloid malignancies. *Nat Rev Cancer* 2012; **12**: 599–612.
27 Argiropoulos B, Humphries RK. Hox genes in hematopoiesis and leukemogenesis. *Oncogene* 2007; **26**: 6766–6776.
28 Alharbi RA, Pettengell R, Pandha HS, Morgan R. The role of HOX genes in normal hematopoiesis and acute leukemia. *Leukemia* 2013; **27**: 1000–1008.
29 Brun AC, Bjornsson JM, Magnusson M, Larsson N, Leveen P, Ehinger M *et al.* Hoxb4-deficient mice undergo normal hematopoietic development but exhibit a mild proliferation defect in hematopoietic stem cells. *Blood* 2004; **103**: 4126–4133.
30 Lawrence HJ, Christensen J, Fong S, Hu YL, Weissman I, Sauvageau G *et al.* Loss of expression of the Hoxa-9 homeobox gene impairs the proliferation and repopulating ability of hematopoietic stem cells. *Blood* 2005; **106**: 3988–3994.
31 Magnusson M, Brun AC, Miyake N, Larsson J, Ehinger M, Bjornsson JM *et al.* HOXA10 is a critical regulator for hematopoietic stem cells and erythroid/megakaryocyte development. *Blood* 2007; **109**: 3687–3696.

Supplementary Information accompanies this paper on the Leukemia website (http://www.nature.com/leu)

© 2014 Macmillan Publishers Limited

From www.bloodjournal.org by guest on April 19, 2015. For personal use only.

Regular Article

MYELOID NEOPLASIA

Depletion of *Sf3b1* impairs proliferative capacity of hematopoietic stem cells but is not sufficient to induce myelodysplasia

Changshan Wang,[1,2] Goro Sashida,[1,2] Atsunori Saraya,[1,2] Reiko Ishiga,[3] Shuhei Koide,[1,2] Motohiko Oshima,[1,2] Kyoichi Isono,[4] Haruhiko Koseki,[4] and Atsushi Iwama[1,2]

[1]Department of Cellular and Molecular Medicine, Graduate School of Medicine, Chiba University, Chiba, Japan; [2]Japan Science and Technology Corporation, Core Research for Evolutional Science and Technology, Gobancho, Chiyoda-ku, Tokyo, Japan; [3]Chromosome Unit, Central Laboratory, Tokyo Medical University, Tokyo, Japan; and [4]Laboratory for Developmental, RIKEN Research Center for Integrative Medical Sciences, RCAI-IMS, Yokohama, Japan

Key Points

- The level of Sf3b1 expression is critical for the proliferative capacity of hematopoietic stem cells.
- Haploinsufficiency for Sf3b1 is not sufficient to induce a RARS-like phenotype in mice.

Numerous studies have recently reported mutations involving multiple components of the messenger RNA (mRNA) splicing machinery in patients with myelodysplastic syndrome (MDS). *SF3B1* is mutated in 70% to 85% of refractory anemia with ringed sideroblasts (RARS) patients and is highly associated with the presence of RARS, although the pathological role of *SF3B1* mutations in MDS-RARS has not been elucidated yet. Here, we analyzed the function of pre-mRNA splicing factor *Sf3b1* in hematopoiesis. *Sf3b1*$^{+/-}$ mice maintained almost normal hematopoiesis and did not develop hematological malignancies during a long observation period. However, *Sf3b1*$^{+/-}$ cells had a significantly impaired capacity to reconstitute hematopoiesis in a competitive setting and exhibited some enhancement of apoptosis, but they did not show any obvious defects in differentiation. Additional depletion of *Sf3b1* with shRNA in *Sf3b1*$^{+/-}$ hematopoietic stem cells (HSCs) severely compromised their proliferative capacity both in vitro and in vivo. Finally, we unexpectedly found no changes in the frequencies of sideroblasts in either *Sf3b1*$^{+/-}$ erythroblasts or cultured *Sf3b1*$^{+/-}$ erythroblasts expressing shRNA against *Sf3b1*. Our findings indicate that the level of *Sf3b1* expression is critical for the proliferative capacity of HSCs, but the haploinsufficiency for *Sf3b1* is not sufficient to induce a RARS-like phenotype. (*Blood*. 2014; 123(21):3336-3343)

Introduction

Alternative pre-messenger RNA (mRNA) splicing is a key regulator of biological diversity and the normal gene expression in higher eukaryotes.[1] More than 90% of multiple-exon genes undergo multiple alternative splicing events within the same transcript.[2,3] Nuclear pre-mRNA splicing is catalyzed by the spliceosome, a multimegadalton ribonucleoprotein (RNP) complex comprised of 5 small nuclear (sn)RNPs and numerous proteins. SF3B1 is a core component of the splicing machinery, forming the U2 snRNP together with the SF3A complex and the U2 small nuclear RNA. The complete U2 snRNP recognizes the 3′ splice site at intron-exon junctions.[4,5] Of note, recent next-generation sequencing studies have identified several mutations involving multiple components of the mRNA splicing machinery, including *SF3B1*, *SRSF2*, *U2AF1*, *ZRSR2*, *PRPF40B*, *U2AF65*, and *SF1* in myelodysplastic syndrome (MDS) patients.[6-8] Among these MDS patients, *SF3B1* is one of the most frequently mutated genes, and mutations in *SF3B1* have been found in ~80% of patients with refractory anemia with ringed sideroblasts (RARS) and RARS with thrombocytosis.[6] In addition, *SF3B1* mutations have also been identified in 15% of patients with chronic lymphocytic leukemia[9] and at lower frequencies in patients with solid tumors such as melanoma and breast cancer.[10,11]

MDS is a heterogeneous group of myeloid malignancies characterized by impaired hematopoiesis with dysplastic blood cells and a predisposition to the development of acute myeloid leukemia.[12,13] Various mutations have recently been identified in patients with MDS.[14,15] Among these, MDS patients harboring *SF3B1* mutations tend to have mild cytopenia and longer survival than patients without the *SF3B1* mutation.[15] However, it remains unknown how deregulation of SF3B1 is involved in the development of RARS. *SF3B1* mutations are confined to a small region corresponding to exons 14 and 15, where no homozygous mutations have been reported. The presence of hot spots and the absence of nonsense or frameshift changes suggest that *SF3B1* mutations are associated with some neomorphic function rather than loss of function.[6,8] Therefore, it is assumed that depletion of *Sf3b1* alone does not recapitulate the pathophysiological consequences of *SF3B1* mutations in MDS cells. To address this question, we analyzed the function of Sf3b1 in hematopoiesis utilizing *Sf3b1* heterozygous mice, because *Sf3b1* null homozygote mice die at around the 16- to 32-cell stage during preimplantation development.[16] *Sf3b1* heterozygous mice develop normally except for mild skeletal homeotic changes due to deregulated *Hox* gene expression.[16]

Submitted December 17, 2013; accepted April 9, 2014. Prepublished online as *Blood* First Edition paper, April 15, 2014; DOI 10.1182/blood-2013-12-544544.

The online version of this article contains a data supplement.

The publication costs of this article were defrayed in part by page charge payment. Therefore, and solely to indicate this fact, this article is hereby marked "advertisement" in accordance with 18 USC section 1734.

© 2014 by The American Society of Hematology

From www.bloodjournal.org by guest on April 19, 2015. For personal use only.

We found that haploinsufficiency for *Sf3b1* significantly impairs the repopulating capacity of hematopoietic stem cells (HSCs) in vivo, but does not induce MDS-like phenotypes such as the appearance of RARs. Additional depletion of *Sf3b1* by RNA interference further compromised the proliferative capacity of *Sf3b1*$^{+/-}$ HSCs both in vitro and in vivo. Our findings show that the level of *Sf3b1* expression is critical for the proliferative capacity of HSCs and that the partial loss of *Sf3b1* is not sufficient to develop MDS in vivo.

Materials and Methods

Mice

Sf3b1 heterozygous mice were generated as previously described.[16] C57BL/6 mice congenic for the Ly5 locus (CD45.1) were purchased from Sankyo-Laboratory Service. All experiments using mice were performed in accordance with our institutional guidelines for the use of laboratory animals and approved by the Review Board for Animal Experiments of Chiba University (approval ID: 25-104).

Flow cytometry and antibodies

Monoclonal antibodies (mAbs) recognizing the following antigens were used in flow cytometry and cell sorting: CD45.2 (104), CD45.1 (A20), Gr-1 (RB6-8C5), CD11b/Mac-1 (M1/70), Ter-119, CD127/IL-7Rα (A7R34), B220 (RA3-6B2), CD4 (L3T4), CD8α (53-6.7), CD43 (S7), IgM (1B4B1), CD117/c-Kit (2B8), Sca-1 (D7), and CD16/32/FcγRII-III (93). The mAbs were purchased from BD BioSciences (San Jose, CA), eBioScience (San Diego, CA), or BioLegend (San Diego, CA). Dead cells were eliminated by staining with propidium iodide (1 μg/mL, Sigma). All flow cytometric analyses and cell sorting were performed on a JSAN (Bay Bioscience, Kobe, Japan), FACSAria II, or FACSCanto II (BD Biosciences).

Purification of hematopoietic cells

Hematopoietic cells were harvested from long bones that were triturated and passed through 40-μm nylon mesh to obtain a single cell suspension. Mononuclear cells (MNCs) were isolated on Ficoll-Paque PLUS (GE Healthcare, Buckinghamshire, UK) and incubated with a mixture of biotin-conjugated mAbs against lineage markers, including Gr-1, Mac-1, Ter-119, B220, IL-7Rα, CD4, and CD8α. The cells were further stained with allophycocyanin (APC)-Cy7-conjugated streptavidin and a combination of mAbs, including fluorescein isothiocyanate-conjugated anti-CD34, phycoerythrin (PE)- or PE-Cy7-Sca-1, PE-FcγR, and APC-c-Kit. Pacific Blue-CD45.2 mAb was used as an additional marker for donor-derived cells in the bone marrow (BM) of B6-CD45.1 recipient mice. HSC ($Lin^-CD34^{-/low}c\text{-}Kit^+Sca\text{-}1^+$), multipotent progenitor (MPP) ($Lin^-CD34^+c\text{-}Kit^+Sca\text{-}1^+$), common myeloid progenitor ($Lin^-Sca\text{-}1^-c\text{-}Kit^+CD34^+Fc\gamma R^{low}$), granulocyte/macrophage progenitor ($Lin^-Sca\text{-}1^-c\text{-}Kit^+CD34^+Fc\gamma R^{hi}$), and megakaryocyte/erythroid progenitor (MEP) ($Lin^-Sca\text{-}1^-c\text{-}Kit^+CD34^-Fc\gamma R^{low}$) fractions were defined as previously described.[17,18]

BM transplantation

BM cells (2×10^6) from CD45.2 mutant mice (test cells) were transplanted intravenously into 8-week-old CD45.1 recipients irradiated at a dose of 9.5 Gy with or without the same number of BM cells from 8-week-old CD45.1 congenic mice (competitor cells). At 3 months after transplantation, serial transplants were carried out by transferring 2×10^6 BM cells to secondary recipients. The chimerism of donor-derived hematopoiesis was monitored monthly by flow cytometry. Peripheral blood (PB) cells were stained with a mixture of mAbs that included PE-anti-Gr-1, PE-anti-Mac-1, APC-anti-B220, APC-Cy7-anti-CD4, APC-Cy7-anti-CD8α, fluorescein isothiocyanate-CD45.2, and PE-Cy7-anti-CD45.1. The proportion of donor cells was evaluated by dividing the number of CD45.2-single positive cells by the total number of CD45-positive cells (CD45.1 + CD45.2).

Homing assay

Wild-type (WT) and *Sf3b1*$^{+/-}$ BM MNCs (10^6 cells) were labeled with 5 μM carboxyfluorescein diacetate, succinimidyl ester (CFSE, Molecular Plobes) in phosphate-buffered saline at 37°C for 10 minutes. The cells were then transplanted via tail vein. After 8 hours, recipient BM cells were isolated and analyzed for $CFSE^+$ cells with a FACSCanto II (Beckton Dickinson).

Knockdown of *Sf3b1*

For knockdown of *Sf3b1*, pCS-H1-shRNA-EF-1-EGFP was used.[19] Target sequences were as follows; *Sh-Sf3b1*#525; GAGCTAAAGCTGGA GAACTA and *Sh-Sf3b1*#1282; GCTCGAAAGCTGACAGCAA. $CD34^-$KSL HSCs were transduced with the indicated lentivirus as previously described with minor modifications.[20] $CD34^-$KSL HSCs were sorted into 96-well microtiter plates coated with the recombinant human fibronectin fragment CH-296 (RetroNectin; Takara Shuzo) at 100 cells per well and then incubated in α- minimum essential medium supplemented with 1% fetal bovine serum (FBS), 1% L-glutamine, penicillin, streptomycin solution (GPS; Sigma-Aldrich), 50 μM 2-mercaptoethanol (2-ME), 100 ng/mL mouse stem cell factor (SCF; PeproTech), and 100 ng/mL human thrombopoietin (TPO; PeproTech) for 24 hours. Next, cells were transduced with the indicated virus at a multiplicity of infection of 1500 in the presence of 1 μg/mL RetroNectin and 10 μg/mL protamine sulfate (Sigma-Aldrich) for 24 hours. After transduction, cells were further incubated in S-Clone SF-O3 (Sanko Junyaku) supplemented with 0.2% bovine serum albumin, 50 μM 2-ME, 1% GPS, 50 ng/mL SCF, and 50 ng/mL TPO for 2.5 days, and then subjected to competitive repopulation assays. For in vitro proliferation assay, infected cells were further incubated in S-Clone SF-O3 supplemented with 0.2% bovine serum albumin, 50 μM 2-ME, 1% GPS, 50 ng/mL SCF, and 50 ng/mL TPO for 14 days. The transduction efficiency was 60% to 90%, as judged from green fluorescent protein (GFP) expression. To induce knockdown in erythroblasts, $c\text{-}Kit^+$ progenitors preincubated in Iscove modified Dulbecco medium supplemented with 10% FBS and 50 ng/mL of SCF, TPO, and FP6 (kindly provided by Kyowa Hakko Kirin Pharma, Inc.) and 40 ng/mL interleukin-3 (IL-3; PeproTech) were similarly transduced with the indicated virus at a multiplicity of infection of 20. At 24 hours posttransduction, cells were cultured for 3 days in Iscove modified Dulbecco medium supplemented with 10% FBS and 50 units/mL of human erythropoietin (EPO; kindly provided by Kyowa Hakko Kirin) then subjected to cell sorting to recover the GFP^+CD71^+ transduced erythroblasts.

Microarray analysis

Total RNA was extracted from pooled BM $lineage^-Sca\text{-}1^+c\text{-}Kit^+$ (LSK) cells (isolated from 4-5 mice per each genotype) by using an RNeasy Plus Mini Kit (Qiagen). Microarray analysis using a SurePrint G3 Mouse GE Microarray 8x60K kit (Agilent) was carried out as previously described.[21] The raw data were deposited in Gene Expression Omnibus under the accession number GSE51038.

Real-time quantitative RT-PCR

Total RNA was isolated using TRIZOL LS solution (Invitrogen) and reverse-transcribed by the ThermoScript RT-PCR system (Invitrogen) with an oligo-dT primer. Real-time quantitative reverse-transcription polymerase chain reaction (RT-PCR) was performed with an ABI Prism 7300 Thermal Cycler (Applied Biosystems) using FastStart Universal Probe Master (Roche) and the indicated combinations of Universal Probe Library (Roche). Primer sequences are as follows:

Gene/Forward/Reverse primer (5′ to 3′)/probe
Sf3b1 agcaagctcgtggatgatg/ccacaggttattatgaccaagaaa/#31
Hprt1 tcttcctcagaccgctttt/cctggttcatcatcgctaatc/#95
Mycn tgtgtctgttccagctactgc/ ttcctcctcgtcatcctcat/#68
Gdf15 gagctacggggtcgcttc/ gagtcctctcggctctggt/#62
Epx tcagcaagtgagaaggatcg/ agcgtctccaggcattgtat/#97
Ear2 gggagccacaaagcagac/ ttgatatgctggatggcaaa/#48
Cd83 tggttctgaaggtgacagga/ caaccagagagaagagcaacac/#29
Bcl2a1d tttccagttttgtggcagaat/ tcaaacttctttatgaagccatctt/#2
Blnk tcccatttaattcgacgtttg/ agcataccagggcttaccg/#75
Skil agtgtcttacccagacgtctcac/ agcagactcagatttctttctacttgt/#68

From www.bloodjournal.org by guest on April 19, 2015. For personal use only.

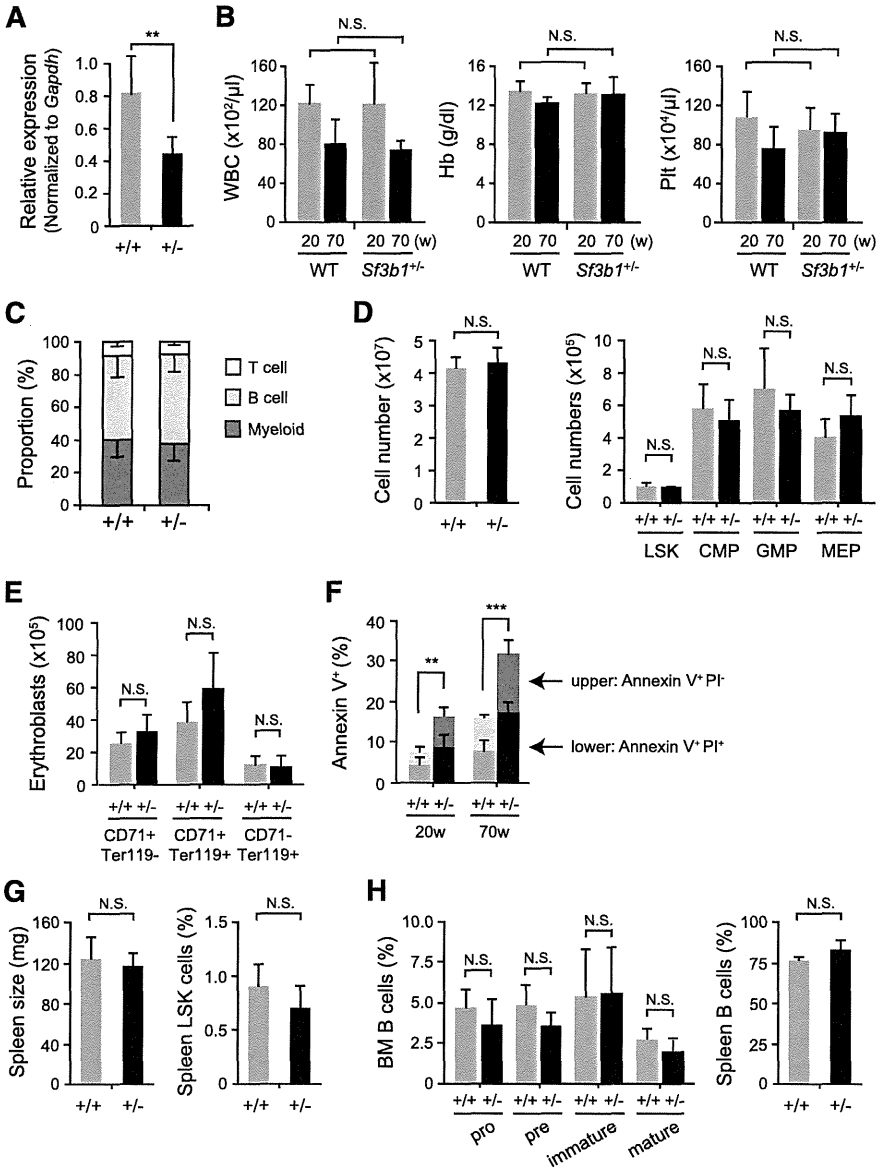

Figure 1. Minimal defects of hematopoiesis in *Sf3b1* heterozygous mice. (A) Quantitative RT-PCR analysis of the expression of *Sf3b1* in LSK cells from WT and $Sf3b1^{+/-}$ mice. *Gapdh* was used to normalize the amount of input RNA. Data are shown as the mean ± standard deviation (SD) for triplicate analyses. (B) PB cell counts in 20- and 70-week-old WT and $Sf3b1^{+/-}$ mice. White blood cell (WBC), hemoglobin (Hb), and platelet (Plt) counts are presented as mean ± SD (WT n = 4; $Sf3b1^{+/-}$ n = 5). (C) The proportion of each cell lineage in PB from 70-week-old WT and $Sf3b1^{+/-}$ mice shown as mean ± SD (WT n = 4; $Sf3b1^{+/-}$ n = 5). (D) Absolute numbers of total MNCs, LSK cells, and myeloid progenitors in a unilateral femur and tibia from 70-week-old WT and $Sf3b1^{+/-}$ mice. Data are shown as the mean ± SD (WT n = 4; $Sf3b1^{+/-}$ n = 5). (E) Absolute numbers of $CD71^+Ter119^-$, $CD71^+Ter119^+$, and $CD71^-Ter119^+$ erythroblasts in a unilateral femur and tibia from WT and 70-week-old $Sf3b1^{+/-}$ mice. Data are shown as the mean ± SD (WT n = 4; $Sf3b1^{+/-}$ n = 5). (F) Percentage of $AnnexinV^+PI^-$ and $AnnexinV^+PI^+$ apoptotic cells in BM LSK cells from 70-week-old WT and $Sf3b1^{+/-}$ mice. Data are shown as the mean ± SD (WT n = 4; $Sf3b1^{+/-}$ n = 5). (G) Size of the spleen and the proportion of LSK cells in the spleen from 32-week-old WT and $Sf3b1^{+/-}$ mice. Data are shown as the mean ± SD (WT n = 5; $Sf3b1^{+/-}$ n = 5). (H) B-cell differentiation in the BM and proportion of B cells in the spleen from 32-week-old WT and $Sf3b1^{+/-}$ mice. The proportion of Pro-B ($B220^+CD43^+IgM^-$), Pre-B ($B220^+CD43^-IgM^-$), and immature B ($B220^+CD43^-IgM^+$) and mature B ($B220^{hi}CD43^-IgM^+$) cells in BM is shown as the mean ± SD (WT n = 5; $Sf3b1^{+/-}$ n = 5). $^*P < .05$; $^{**}P < .01$. N.S., not significant.

Statistical analysis

Statistical significance was analyzed with Student *t* test. The level of significance was set at 0.05.

Results

Minimal defects of hematopoiesis in *Sf3b1* heterozygous mice

Given that *Sf3b1*-deficient mice die at a very early embryonic stage,[16] we first examined hematopoiesis in *Sf3b1* heterozygous ($Sf3b1^{+/-}$) mice that show almost normal development compared with the WT littermates (data not shown). We confirmed that $Sf3b1^{+/-}$ mice exhibited a 40% reduction in the expression of *Sf3b1* in LSK hematopoietic stem/progenitor cells (HSPCs) (Figure 1A). $Sf3b1^{+/-}$ mice did not show any significant changes in white blood cell counts, hemoglobin levels, or platelet counts in their PB at any time points up to 70 weeks old (Figure 1B). $Sf3b1^{+/-}$ mice had a lineage composition of PB MNCs comparable with that of WT mice (Figure 1C). In addition, $Sf3b1^{+/-}$ mice had total BM cell counts comparable with those of WT mice and did not show any significant changes in the numbers of LSKs, common myeloid progenitors, granulocyte/macrophage progenitors, and megakaryocyte/erythroid progenitors (Figure 1D). Consistent with the absence of anemia in $Sf3b1^{+/-}$ mice, $Sf3b1^{+/-}$ mice showed almost normal differentiation of erythroid lineage cells in the BM (Figure 1E). Furthermore, they did not develop any hematological disorders, including MDS by 70 weeks of age (data not shown). Of note, however, $Sf3b1^{+/-}$ mice showed a mild but significant increase in apoptosis in LSK cells compared with WT mice (Figure 1F), though the number of LSK cells did not change in $Sf3b1^{+/-}$ mice. Thus, $Sf3b1^{+/-}$ mice do not show obvious phenotypic changes in hematopoiesis except for mildly enhanced apoptosis.

$Sf3b1^{+/-}$ mice showed no sign of extramedullary hematopoiesis as judged by the normal spleen size and no increase in LSK cells in the spleen (Figure 1G). In addition, $Sf3b1^{+/-}$ mice showed almost normal differentiation and expansion of B cells in the BM and spleen

From www.bloodjournal.org by guest on April 19, 2015. For personal use only.

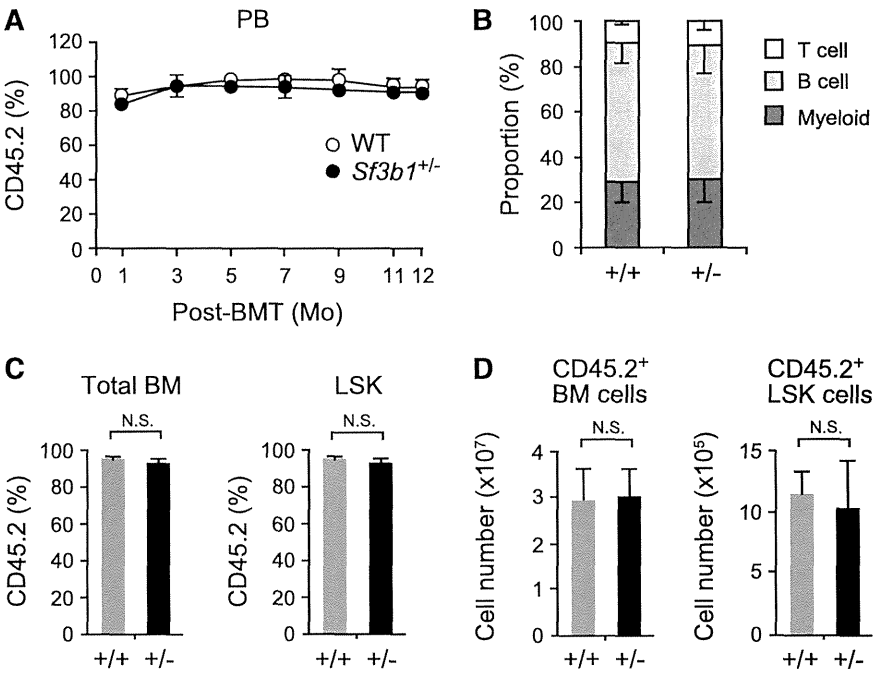

Figure 2. *Sf3b1*$^{+/-}$ BM cells normally reconstitute hematopoiesis in vivo. (A) Contribution of donor cells to PB hematopoiesis. WT and *Sf3b1*$^{+/-}$ BM cells (5×10^6 cells, CD45.2$^+$) were transplanted into lethally irradiated recipient (CD45.1$^+$) mice. Chimerism of donor-derived CD45.2$^+$ cells in the PB is shown as mean ± SD (n = 7). BMT, BM transplant. (B) Lineage contribution of WT and *Sf3b1*$^{+/-}$ donor cells in PB. The proportion of each cell lineage in donor-derived CD45.2$^+$ cells in the PB at 12 months posttransplantation. (C-D) Contribution of donor cells to BM hematopoiesis. Chimerism of donor-derived CD45.2$^+$ cells in total BM cells and LSK cells is shown as mean ± SD (n = 7) in C. Absolute numbers of donor-derived CD45.2$^+$ BM cells and LSK cells are shown as mean ± SD (n = 7) in D. N.S., not significant.

(Figure 1H). These findings indicate that *Sf3b1* haploinsufficiency is not sufficient to induce MDS or clonal expansion of B lymphoid cells in vivo.

Sf3b1 haploinsufficiency results in impaired competitive reconstitution capacity of HSCs

To exclude any effects of reduced *Sf3b1* expression in nonhematopoietic cells in vivo, we next transplanted 5×10^6 WT and *Sf3b1*$^{+/-}$ BM cells (CD45.2$^+$) into lethally irradiated recipient (CD45.1$^+$) mice. *Sf3b1*$^{+/-}$ hematopoietic cells efficiently reconstituted hematopoiesis of recipient mice at least up to 12 months posttransplantation (Figure 2A) and contributed to myeloid and lymphoid cells in PB in a manner similar to WT hematopoietic cells (Figure 2B). *Sf3b1*$^{+/-}$ hematopoietic cells also reconstituted BM cells, including LSK cells to levels comparable with WT cells in proportion (Figure 2C) as well as in absolute number (Figure 2D). Reconstitution of myeloid progenitors and erythroid lineage cells in BM was also comparable between WT and *Sf3b1*$^{+/-}$ mice (data not shown). These findings confirm that haploinsufficiency of *Sf3b1* in hematopoietic cells does not largely impair hematopoiesis. Once again, we did not find any hematological features of MDS in mice reconstituted with *Sf3b1*$^{+/-}$ BM cells up to 1 year postransplantation.

We next performed competitive reconstitution assays utilizing *Sf3b1*$^{+/-}$ (CD45.2$^+$) BM cells together with an equal number of CD45.1$^+$ competitor BM cells to test whether functional defects in *Sf3b1*$^{+/-}$ HSCs become obvious under stressful conditions. *Sf3b1*$^{+/-}$ cells showed significantly less contribution to the PB of recipient mice at all time points compared with WT cells, and their contribution gradually declined over time (Figure 3A). Eventually, chimerism of *Sf3b1*$^{+/-}$ cells declined to very low levels in both PB and BM hematopoietic cells and in BM LSK cells (Figure 3A-B).

To evaluate the reconstitution capacity of *Sf3b1*$^{+/-}$ HSCs more precisely, we performed serial transplantation assays using 2×10^6 whole BM cells from the primary recipient mice. As in Figure 3A, chimerism of *Sf3b1*$^{+/-}$ cells in total MNCs and myeloid cells in PB was significantly less than WT even in the primary recipients (Figure 3A) and further declined in the secondary recipients (Figure 3C). However, *Sf3b1*$^{+/-}$ cells did not show obvious defects in differentiation, because there were no significant changes in the proportion of myeloid and lymphoid lineage cells within CD45.2$^+$ *Sf3b1*$^{+/-}$ cells compared with WT cells (data not shown). To explore

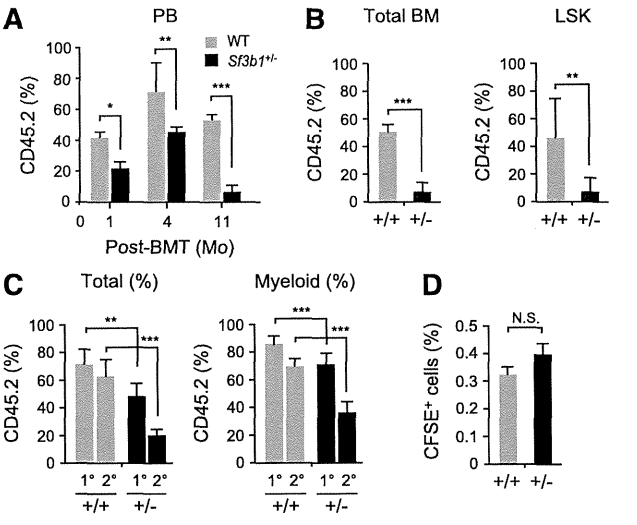

Figure 3. *Sf3b1* haploinsufficiency causes impaired competitive repopulating capacity of HSCs. (A) Contribution of donor cells to PB hematopoiesis. WT and *Sf3b1*$^{+/-}$ BM cells (2×10^6 cells, CD45.2$^+$) together with an equal number of CD45.1$^+$ competitor BM cells were transplanted into lethally irradiated recipient (CD45.1$^+$) mice. Chimerism of donor-derived CD45.2$^+$ cells in the PB is shown as mean ± SD (n = 5). (B) Chimerism of donor-derived CD45.2$^+$ cells in total BM cells and LSK cells at 11 months posttransplantation shown as mean ± SD (n = 5). (C) Serial transplantation assays. WT and *Sf3b1*$^{+/-}$ BM cells (2×10^6 cells, CD45.2$^+$) together with an equal number of CD45.1$^+$ competitor BM cells were transplanted into lethally irradiated recipient (CD45.1$^+$) mice. At 4 months posttransplantation, 2×10^6 whole BM cells from the primary recipient mice were transplanted into the secondary recipient mice. Chimerism of donor-derived CD45.2$^+$ cells was detected in total MNCs and myeloid cells in the PB at 4 months postprimary (1°) and -secondary (2°) transplantation and is shown as mean ± SD (n = 9). (D) Homing assays. CFSE-labeled WT and *Sf3b1*$^{+/-}$ BM MNCs (10^6 cells) were transplanted into lethally irradiated mice. Frequencies of CFSE$^+$ cells detected in BM at 8 hours posttransplantation are shown as mean ± SD (n = 5). *$P < .05$; **$P < .01$; ***$P < .001$. N.S., not significant.

From www.bloodjournal.org by guest on April 19, 2015. For personal use only.

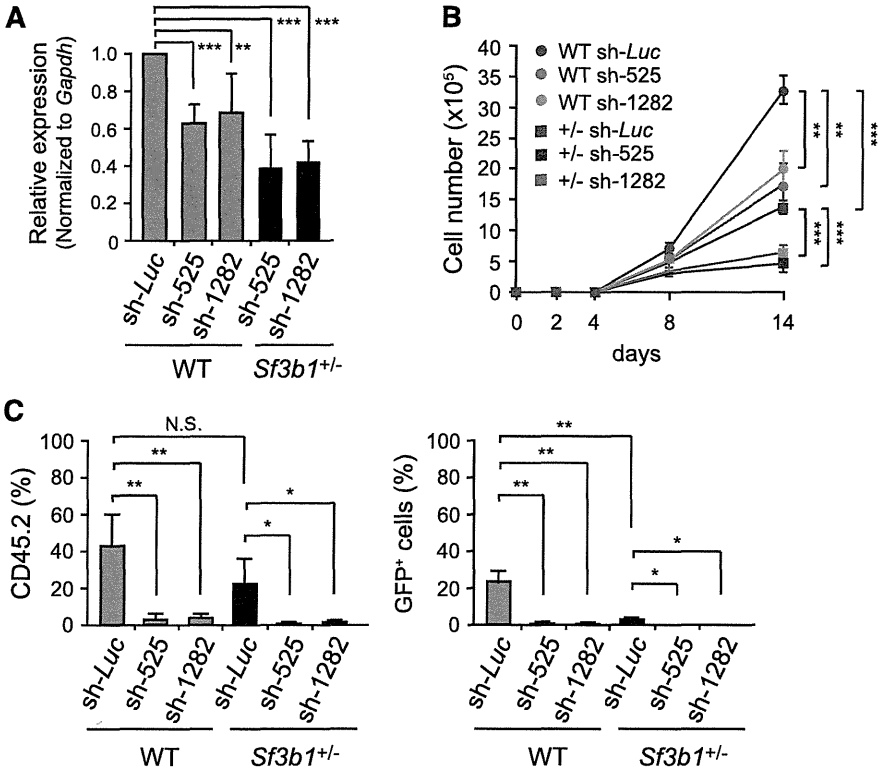

Figure 4. Knockdown of *Sf3b1* compromises proliferative capacity of HSCs. (A) Knockdown efficiencies of shRNAs against *Sf3b1*. WT and $Sf3b1^{+/-}$ LSK cells were transduced with the indicated shRNAs and cultured in the presence of SCF and TPO. At day 3 postinfection, $GFP^+Lin^-c\text{-}Kit^+$ cells were purified by cell sorting, and the levels of *Sf3b1* were analyzed by quantitative RT-PCR analysis. mRNA levels were normalized to *Gapdh* expression. Expression levels relative to that in the control cells transduced with an shRNA against *Luciferase* are shown as the mean ± SD for triplicate analyses. (B) Growth of WT and $Sf3b1^{+/-}$ $CD34^-LSK$ HSCs upon knockdown of *Sf3b1* in culture. One hundred WT and $Sf3b1^{+/-}$ HSCs were transduced with the indicated shRNAs and cultured in the presence of SCF and TPO. Data are shown as mean ± SD (n = 5). The transduction efficiency was ~80% as detected by GFP expression on flow cytometry. (C) Reconstitution capacity of WT and $Sf3b1^{+/-}$ $CD34^-LSK$ HSCs upon knockdown of *Sf3b1* in vivo. WT and $Sf3b1^{+/-}$ HSCs were transduced with the indicated shRNAs as in (B), and 100 transduced HSCs were transplanted into lethally irradiated recipient ($CD45.1^+$) mice together with 2×10^5 $CD45.1^+$ competitor BM cells. Data are shown as mean ± SD (n = 5). Chimerism of donor-derived $CD45.2^+$ cells (left panel) and $CD45.2^+GFP^+$ transduced cells (right panel) in the PB at 4 months posttransplantation are shown as mean ± SD (n = 5). $^*P < .02$; $^{**}P < .01$; $^{***}P < .001$.

whether compromised homing capability may account for the impaired reconstitution capacity of $Sf3b1^{+/-}$ hematopoietic cells, we performed in vivo homing assay utilizing CFSE-labeled WT and $Sf3b1^{+/-}$ BM MNCs. There were no significant differences in the proportion of CFSE-positive cells in the BM at 8 hours postinjection (Figure 3D), indicating that $Sf3b1^{+/-}$ cells retain normal homing capability. Taken together, these findings indicate that *Sf3b1* haploinsufficiency significantly impairs the competitive reconstitution capacity of HSCs.

Level of *Sf3b1* is critical for the proliferative capacity of HSCs

We next examined the effects of further down-regulation of *Sf3b1* on HSCs. To do so, we prepared shRNAs directed to *Sf3b1* (525 and 1282). Transduction efficiency was ~80% as detected by GFP expression on flow cytometry, and no significant difference was observed in transduction efficiencies among samples. Quantitative RT-PCR confirmed that *Sf3b1* levels were reduced by 40% and 60% in WT and $Sf3b1^{+/-}$ LSK cells transduced with shRNA against *Sf3b1*, respectively (Figure 4A). We then transduced $CD34^-$ LSK HSCs with these viruses. We first evaluated the growth of HSCs in liquid culture supplemented only with SCF and TPO, a condition that supports the growth of immature HSPCs rather than their differentiation. Under these conditions, $Sf3b1^{+/-}$ HSCs showed significant growth retardation compared with WT HSCs, and depletion of *Sf3b1* by shRNAs further attenuated their growth compared with the controls expressing shRNA directed to *Luciferase* (Figure 4B). We next transplanted WT and $Sf3b1^{+/-}$ HSCs transduced with shRNAs against *Sf3b1* together with radio-protective $CD45.1^+$ BM cells into lethally irradiated $CD45.1^+$ recipient mice. Depletion of *Sf3b1* severely impaired reconstitution capacity of both WT and $Sf3b1^{+/-}$ HSCs (Figure 4C). The effect of *Sf3b1* knockdown was more obvious in $Sf3b1^{+/-}$ HSCs compared with WT HSCs, showing a clear dependency of reconstitution capacity of HSCs on *Sf3b1* levels. In contrast, we did not see any obvious defects in the differentiation of HSCs, including erythroblasts in BM upon depletion of *Sf3b1* (data not shown). These findings imply that Sf3b1 is required for the self-renewal capacity of HSCs but is not critical for the differentiation capabilities of HSCs.

Sf3b1 haploinsufficiency does not activate the nonsense–mediated mRNA decay pathway

To understand the molecular mechanism through which *Sf3b1* haploinsufficiency affects the function of HSCs, we performed gene expression analysis using LSK HSPCs isolated from 11-month-old WT and $Sf3b1^{+/-}$ mice. We also harvested LSK cells from recipient mice reconstituted with WT and $Sf3b1^{+/-}$ cells at 9 months posttransplantation. Microarray analysis revealed that more genes were altered by >2-fold in $Sf3b1^{+/-}$ LSK cells from primary recipient mice compared with those from 11-month-old mice (Figure 5A; supplemental Table 1, available on the *Blood* Web site). Among these, 12 and 27 genes were up- and down-regulated, respectively, in both analyses. Expression of a portion of genes was validated by quantitative RT-PCR (supplemental Figure 1). Unexpectedly, however, these genes did not include those known to be involved in the regulation of HSC functions.

In contrast, gene set enrichment analysis[22] revealed a number of differences in canonical pathways in gene expression profiles between WT and $Sf3b1^{+/-}$ LSK cells. Many gene sets were commonly enriched in $Sf3b1^{+/-}$ LSK cells isolated from 11-month-old mice and recipient mice at 9 months posttransplantation. Those included gene sets related to transcription, translation, cell cycle and metabolism (supplemental Table 2). Among these, the gene set for the non-sense–mediated mRNA decay (NMD) pathway was negatively enriched in $Sf3b1^{+/-}$ LSK cells, particularly those from primary recipient mice (Figure 5B; supplemental Table 2). NMD is a surveillance pathway that surveys and degrades abnormal transcripts

From www.bloodjournal.org by guest on April 19, 2015. For personal use only.

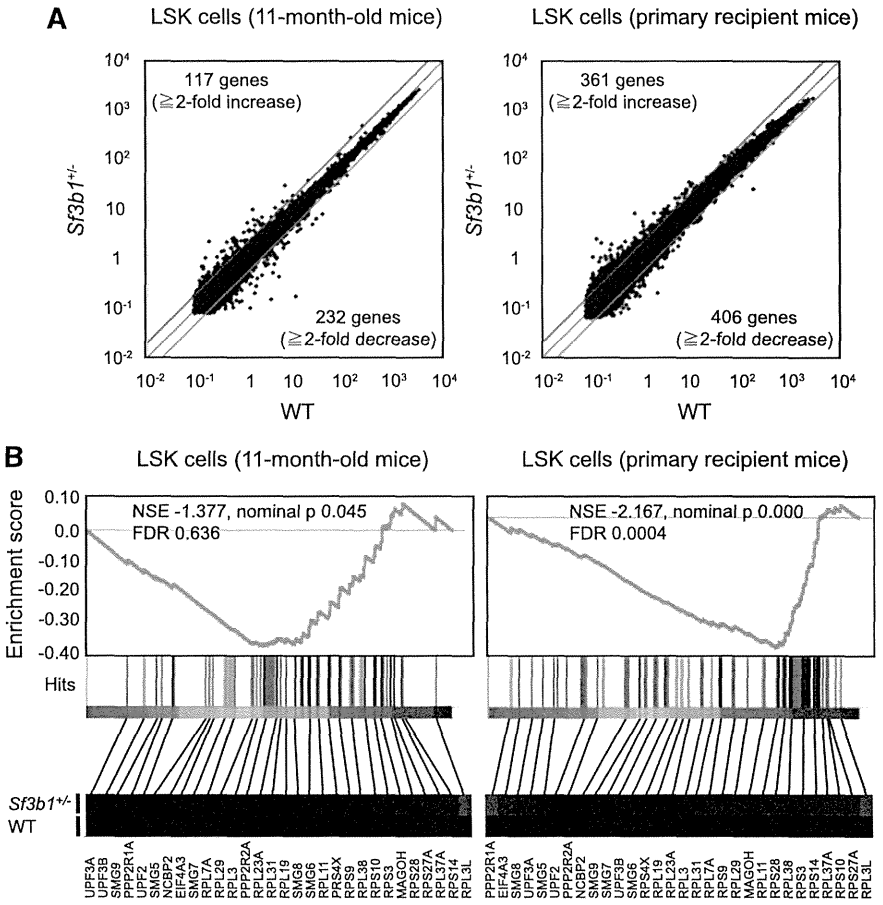

Figure 5. *Sf3b1* haploinsufficiency does not activate the NMD pathway. (A) A scatter diagram of microarray analysis. WT and *Sf3b1*$^{+/-}$ LSK cells were isolated from 11-month-old WT and *Sf3b1*$^{+/-}$ mice and recipient mice reconstituted with WT and *Sf3b1*$^{+/-}$ BM cells at 9 months posttransplantation and then analyzed by microarray-based expression analysis. The average signal levels of *Sf3b1*$^{+/-}$ cells compared with those of WT cells are plotted. The red and green lines represent the borderline for 2-fold increase and 2-fold decrease, respectively, and the numbers of genes altered by >2-fold are indicated. (B) The gene set enrichment analysis demonstrating a significant negative enrichment of the NMD pathway genes in *Sf3b1*$^{+/-}$ LSK cells relative to WT LSK cells. Normalized enrichment scores (NSE), nominal *P* values, and false discovery rates (FDRs) are indicated. Red and blue represent positive (up-regulated in the given genotype relative to WT) and negative (up-regulated in WT relative to the given genotype) enrichment, respectively. Heat maps showing the gene expression profiles of 30 randomly selected genes are indicated below the plot.

that contain premature stop codons.[23,24] Because of aberrant splicing, the genes in this pathway, such as *MAGOH*, *SMG6*, *SMG7*, *SMG9*, and *UPF3B*, are activated in HeLa cells overexpressing an U2AF35 mutant identified in MDS patients.[6] Conversely, these NMD pathway genes were expressed at levels comparable with WT LSK cells or mildly down-regulated in *Sf3b1*$^{+/-}$ LSK cells (Figure 5B), and this trend was validated by quantitative RT-PCR (data not shown). These findings indicate that *Sf3b1* haploinsufficiency is not sufficient for activating NMD pathway.

Reduced *Sf3b1* expression is not sufficient to induce RARs

Given that *SF3B1* is very frequently mutated in RARS patients, we finally examined the frequencies of sideroblasts in CD71$^+$ BM erythroblasts from 11-month-old WT and *Sf3b1*$^{+/-}$ mice. Sideroblasts are erythroblasts with granules of iron accumulated in perinuclear mitochondria and are classified according to the WHO International Working Group on Morphology of MDS[25]: type 1 sideroblasts with fewer than 5 siderotic granules in the cytoplasm, Type 2 sideroblasts with 5 or more siderotic granules but not in a perinuclear distribution, and Type 3 or RARs with 5 or more granules in a perinuclear position surrounding the nucleus or encompassing at least one-third of the nuclear circumference. Although a recent study has shown that *Sf3b1*$^{+/-}$ BM cells have a significantly increased number of RARs,[26] we did not detect any RARs in our mice. We found only type 1 sideroblasts at frequencies comparable between WT and *Sf3b1*$^{+/-}$ cells (Figure 6A). To examine whether the level of *Sf3b1* expression is critical for the induction of RARs, we transduced WT and *Sf3b1*$^{+/-}$ c-Kit$^+$ progenitor cells with shRNAs against *Sf3b1* and then cultured them in the presence of EPO to induce erythroblasts (Figure 6B). Again, depletion of *Sf3b1* in erythroblasts in culture did not increase the number of CD71$^+$ sideroblasts compared with the control erythroblasts expressing shRNA against *Luciferase* or induce RARs (Figure 6B-C). Taken together, these findings indicate that the reduction in the levels of Sf3b1 does not cause appearance of RARs that is the definitive dysplastic feature of RARS.

Discussion

Our study demonstrated that heterozygosity for *Sf3b1* does not significantly perturb hematopoiesis except for mildly enhancing apoptosis in HSPCs. It also fails to induce any hematological malignancies, including MDS, within an observation period up to 70 weeks. Nevertheless, *Sf3b1*$^{+/-}$ HSCs showed significantly impaired reconstitution capacity in a competitive setting, and further reduction in *Sf3b1* levels by RNA interference severely compromised the reconstitution capacity of HSCs, though it did not affect their differentiation potential. These findings are consistent with the effect of U2AF35 mutants in HSCs.[6] Exogenous U2AF35 mutants compromised the reconstitution capacity of WT HSCs, suggesting a dominant-negative action of U2AF35 mutants relative to the WT U2AF35 protein. Indeed, there are reported mutational hot spots in U2AF35 in patients with MDS,[6,27] none of which are homozygous, nonsense, or frameshift mutations. All of these findings suggest that mutations in U2AF35 are associated with some gain of function rather than simple loss of function. SF3B1 mutations are assumed to

From www.bloodjournal.org by guest on April 19, 2015. For personal use only.

A Number of sideroblasts in 10^3 erythroblasts in vivo

	Number of siderotic granules					ringed sideroblast
	1	2	3	4	5<	
WT	1.2±1.8	0	0	0	0	0
Sf3b1$^{+/-}$	1.1±1.9	0	0	0	0	0
WT BMT	0.9±1.1	0.9±1.1	0	0	0	0
Sf3b1$^{+/-}$ BMT	2.1±1.4	0.8±1.2	0	0	0	0

B Number of sideroblasts in 10^3 erythroblasts in vitro

	Number of siderotic granules					ringed sideroblast
	1	2	3	4	5<	
WT *Luc*	2.7±4.0	0.9±2.0	0	0	0	0
Sf3b1$^{+/-}$ *Luc*	3.0±2.7	2.7±2.5	0	0	0	0
Sf3b1$^{+/-}$ *525*	3.7±3.7	3.8±4.0	0	0	0	0
Sf3b1$^{+/-}$ *1282*	3.5±2.1	1.0±2.2	0	1.0±2.2	0	0

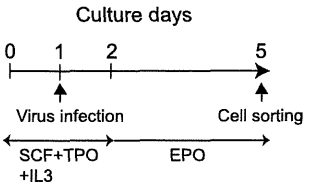

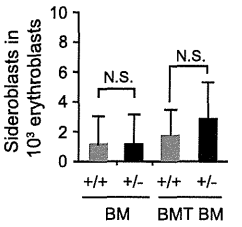

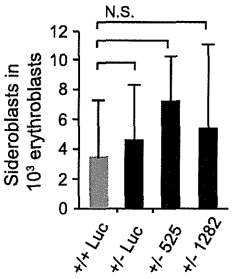

C

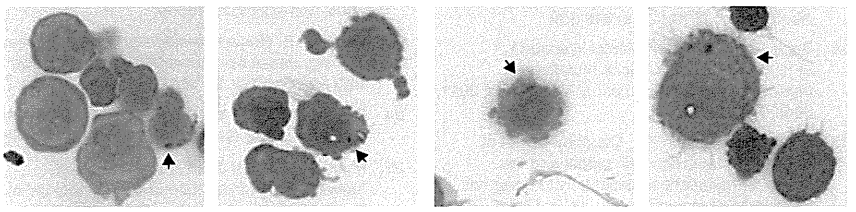

Figure 6. Reduced *Sf3b1* expression is not sufficient to induce RARs. (A) Frequencies of sideroblastic erythroblasts in *Sf3b1*$^{+/-}$ erythroblasts. CD71$^+$ erythroblasts in BM of WT and *Sf3b1*$^{+/-}$ mice and recipients repopulated with WT and *Sf3b1*$^{+/-}$ BM cells at 11 months posttransplantation (WT BMT and *Sf3b1*$^{+/-}$ BMT, respectively) were isolated by cell sorting. The cells were cytospun onto slide glasses, subjected to Prussian Blue staining, and then examined under a light microscope. Numbers of cells with siderotic granules per 1000 erythroblasts are shown in a table and a graph. Data are shown as mean ± SD. Counts of 1000 cells were independently performed 3 times. (B) Frequencies of sideroblastic erythroblasts in *Sf3b1*$^{+/-}$ erythroblasts upon knockdown of *Sf3b1*. c-Kit$^+$ progenitors transduced with shRNA against *Sf3b1* were cultured in the presence of EPO to induce erythroblasts (bottom). GFP$^+$CD71$^+$-transduced erythroblasts were isolated by cell sorting, then evaluated for the presence of sideroblasts in a manner similar to (A). (C) Representative sideroblastic erythroblasts observed in (B). Arrows indicate siderotic granules.

behave in a fashion similar to U2AF35 mutations because of its similar mutational characteristics. Therefore, we are not sure whether the depletion of Sf3b1 that we used in this study precisely reflects the pathophysiological consequences of SF3B1 mutations in MDS cells. However, it is intriguing that both U2AF35 mutants and depletion of Sf3b1 compromised the proliferative capacity of HSCs in a similar fashion. These findings suggest that SF3B1 mutations do not confer a growth advantage to MDS clones over normal hematopoietic cells, thus highlighting the requirement of cooperation with other gene mutations.

As expected from its function in pre-mRNA splicing, RNA sequencing analysis of BM cells from a patient with RARS with an SF3B1 mutation showed alternative splicing in 350 of 9069 genes, including 4 relevant genes to the pathology of MDS such as *ASXL1*, *CBL*, *EZH1*, and *RUNX3*.[26] In addition, the NMD pathway, which surveys and degrades abnormal transcripts, was activated in HeLa cells overexpressing an U2AF35 mutant identified in MDS patients. In contrast, the NMD pathway was suppressed in *Sf3b1*$^{+/-}$ LSK cells in this study, even in LSK cells reconstituted from donor BM cells in recipient mice, suggesting that *Sf3b1* haploinsufficiency does not cause abnormal RNA splicing sufficient for activating the NMD pathway. Nonetheless, *Sf3b1*$^{+/-}$ HSCs showed impaired reconstitution capacity in vivo and growth retardation in culture. It is possible that *Sf3b1* haploinsufficiency induces subclinical levels of splicing abnormalities that cause impairment in HSC functions only under stressful conditions such as transplant and in vitro culture and that mild but significant levels of altered gene expression detected in microarray analyses could be attributed to the splicing defect.

Notably, we did not detect any changes in the frequencies of sideroblasts and did not detect RARs in *Sf3b1*$^{+/-}$ BM cells and *Sf3b1*$^{+/-}$ erythroblasts depleted of *Sf3b1*. Down-regulation of *ABCB7* and overexpression of *MITOCHONDRIAL FERRITIN* (*FTMT*) in immature red cells are typical features of RARS.[28] We analyzed the expression of *Abcb7* and *Ftmt* in *Sf3b1*$^{+/-}$ CD71$^+$ Ter119$^+$ erythroblasts and observed no significant changes in *Abcb7* and *Ftmt* expression (data not shown). These results indicate that simple reduction in the levels of Sf3b1 does not cause abnormal iron metabolism in mitochondria and present a striking contrast with the recent report showing an increased frequency of RARs in the same *Sf3b1*$^{+/-}$ BM cells.[26] The difference in the results of the detection of RARs in the same mouse strain using a conventional staining method is obscure but could be partly due to the different conditions under which the mice were maintained. Nevertheless, this point requires further investigation in comparison with the effects of SF3B1 mutants in the induction of RARs. As suggested from the mutational properties of the *SF3B1* gene in MDS, SF3B1 mutants might acquire some aberrant functions, like IDH1/2 mutants in cancer, that lead to dysregulated iron metabolism.[29]

In conclusion, our findings indicate that the level of *Sf3b1* gene expression is critical in the maintenance of proliferative capacity of HSCs. However, heterozygosity for *Sf3b1* alone does not induce apparent RNA splicing abnormalities or lead to the development of

From www.bloodjournal.org by guest on April 19, 2015. For personal use only.

RARS. Further analysis of mice expressing *SF3B1* mutants specifically in hematopoietic cells would promote precise understanding of the pathological function of *SF3B1* mutations in the development of MDS.

Acknowledgments

The authors thank Drs K. Matsushita and K. Kitamura for Prussian Blue staining and members of the Iwama Laboratory for discussion during the preparation of this manuscript, particularly George R. Wendt for a critical reading of the manuscript.

This work was supported in part by Grants-in-Aid for Scientific Research (24249054 and 25130702) and Scientific Research on Innovative Areas "Cell Fate" (22118004) from MEXT, Japan, a Grant-in-Aid for Core Research for Evolutional Science and Technology from the Japan Science and Technology Corporation, and grants from the Uehara Memorial Foundation and the Takeda Science Foundation.

Authorship

Contribution: C.W. performed the experiments, analyzed results, made the figures, and actively wrote the manuscript; G.S., A.S., R.I., S.K., and M.O. assisted with the experiments, including the hematopoietic analyses; K.I. and H.K. provided mice; and A.I. conceived of and directed the project, secured funding, and actively wrote the manuscript.

Conflict-of-interest disclosure: The authors declare no competing financial interests.

Correspondence: Atsushi Iwama, 1-8-1 Inohana, Chuo-ku, Chiba, 260-8670 Japan; e-mail: aiwama@faculty.chiba-u.jp.

References

1. Matlin AJ, Clark F, Smith CWJ. Understanding alternative splicing: towards a cellular code. *Nat Rev Mol Cell Biol.* 2005;6(5):386-398.
2. Wang ET, Sandberg R, Luo S, et al. Alternative isoform regulation in human tissue transcriptomes. *Nature.* 2008;456(7221):470-476.
3. Pan Q, Shai O, Lee LJ, Frey BJ, Blencowe BJ. Deep surveying of alternative splicing complexity in the human transcriptome by high-throughput sequencing. *Nat Genet.* 2008;40(12):1413-1415.
4. Wang C, Chua K, Seghezzi W, Lees E, Gozani O, Reed R. Phosphorylation of spliceosomal protein SAP 155 coupled with splicing catalysis. *Genes Dev.* 1998;12(10):1409-1414.
5. Krämer A, Mulhauser F, Wersig C, Gröning K, Bilbe G. Mammalian splicing factor SF3a120 represents a new member of the SURP family of proteins and is homologous to the essential splicing factor PRP21p of Saccharomyces cerevisiae. *RNA.* 1995;1(3):260-272.
6. Yoshida K, Sanada M, Shiraishi Y, et al. Frequent pathway mutations of splicing machinery in myelodysplasia. *Nature.* 2011;478(7367):64-69.
7. Visconte V, Makishima H, Jankowska A, et al. SF3B1, a splicing factor is frequently mutated in refractory anemia with ring sideroblasts. *Leukemia.* 2012;26(3):542-545.
8. Ogawa S. Splicing factor mutations in myelodysplasia. *Int J Hematol.* 2012;96(4): 438-442.
9. Wan Y, Wu CJ. SF3B1 mutations in chronic lymphocytic leukemia. *Blood.* 2013;121(23): 4627-4634.
10. Harbour JW, Roberson EDO, Anbunathan H, Onken MD, Worley LA, Bowcock AM. Recurrent mutations at codon 625 of the splicing factor SF3B1 in uveal melanoma. *Nat Genet.* 2013; 45(2):133-135.
11. Ellis MJ, Ding L, Shen D, et al. Whole-genome analysis informs breast cancer response to aromatase inhibition. *Nature.* 2012;486(7403): 353-360.
12. Nimer SD. MDS: a stem cell disorder—but what exactly is wrong with the primitive hematopoietic cells in this disease? *Hematology Am Soc Hematol Educ Program.* 2008;43-51.
13. Raza A, Galili N. The genetic basis of phenotypic heterogeneity in myelodysplastic syndromes. *Nat Rev Cancer.* 2012;12(12):849-859.
14. Bejar R, Stevenson K, Abdel-Wahab O, et al. Clinical effect of point mutations in myelodysplastic syndromes. *N Engl J Med.* 2011; 364(26):2496-2506.
15. Bejar R, Stevenson KE, Caughey BA, et al. Validation of a prognostic model and the impact of mutations in patients with lower-risk myelodysplastic syndromes. *J Clin Oncol.* 2012; 30(27):3376-3382.
16. Isono K, Mizutani-Koseki Y, Komori T, Schmidt-Zachmann MS, Koseki H. Mammalian polycomb-mediated repression of Hox genes requires the essential spliceosomal protein Sf3b1. *Genes Dev.* 2005;19(5):536-541.
17. Akashi K, Traver D, Miyamoto T, Weissman IL. A clonogenic common myeloid progenitor that gives rise to all myeloid lineages. *Nature.* 2000; 404(6774):193-197.
18. Osawa M, Hanada K, Hamada H, Nakauchi H. Long-term lymphohematopoietic reconstitution by a single CD34-low/negative hematopoietic stem cell. *Science.* 1996;273(5272):242-245.
19. Katayama K, Wada K, Miyoshi H, et al. RNA interfering approach for clarifying the PPARgamma pathway using lentiviral vector expressing short hairpin RNA. *FEBS Lett.* 2004; 560(1-3):178-182.
20. Iwama A, Oguro H, Negishi M, et al. Enhanced self-renewal of hematopoietic stem cells mediated by the polycomb gene product Bmi-1. *Immunity.* 2004;21(6):843-851.
21. Tanaka S, Miyagi S, Sashida G, et al. Ezh2 augments leukemogenicity by reinforcing differentiation blockage in acute myeloid leukemia. *Blood.* 2012;120(5):1107-1117.
22. Subramanian A, Tamayo P, Mootha VK, et al. Gene set enrichment analysis: a knowledge-based approach for interpreting genome-wide expression profiles. *Proc Natl Acad Sci USA.* 2005;102(43):15545-15550.
23. Maquat LE. Nonsense-mediated mRNA decay: splicing, translation and mRNP dynamics. *Nat Rev Mol Cell Biol.* 2004;5(2):89-99.
24. Faustino NA, Cooper TA. Pre-mRNA splicing and human disease. *Genes Dev.* 2003;17(4):419-437.
25. Mufti GJ, Bennett JM, Goasguen J, et al; International Working Group on Morphology of Myelodysplastic Syndrome. Diagnosis and classification of myelodysplastic syndrome: International Working Group on Morphology of myelodysplastic syndrome (IWGM-MDS) consensus proposals for the definition and enumeration of myeloblasts and ring sideroblasts. *Haematologica.* 2008;93(11):1712-1717.
26. Visconte V, Rogers HJ, Singh J, et al. SF3B1 haploinsufficiency leads to formation of ring sideroblasts in myelodysplastic syndromes. *Blood.* 2012;120(16):3173-3186.
27. Graubert TA, Shen D, Ding L, et al. Recurrent mutations in the U2AF1 splicing factor in myelodysplastic syndromes. *Nat Genet.* 2012; 44(1):53-57.
28. Nikpour M, Scharenberg C, Liu A, et al. The transporter *ABCB7* is a mediator of the phenotype of acquired refractory anemia with ringed sideroblasts. *Leukemia.* 2013;27:889-896.
29. Figueroa ME, Abdel-Wahab O, Lu C, et al. Leukemic IDH1 and IDH2 mutations result in a hypermethylation phenotype, disrupt TET2 function, and impair hematopoietic differentiation. *Cancer Cell.* 2010;18(6):553-567.

nature COMMUNICATIONS

ARTICLE

Received 24 Sep 2013 | Accepted 21 May 2014 | Published 23 Jun 2014

DOI: 10.1038/ncomms5177

Ezh2 loss promotes development of myelodysplastic syndrome but attenuates its predisposition to leukaemic transformation

Goro Sashida[1,2], Hironori Harada[3,†], Hirotaka Matsui[4], Motohiko Oshima[1,2], Makiko Yui[1,2], Yuka Harada[5,†], Satomi Tanaka[1,6], Makiko Mochizuki-Kashio[1,2], Changshan Wang[1,2], Atsunori Saraya[1,2], Tomoya Muto[1,6], Yoshihiro Hayashi[7,8], Kotaro Suzuki[9], Hiroshi Nakajima[9], Toshiya Inaba[4], Haruhiko Koseki[2,10], Gang Huang[7,8], Toshio Kitamura[11] & Atsushi Iwama[1,2]

Loss-of-function mutations of *EZH2*, a catalytic component of polycomb repressive complex 2 (PRC2), are observed in ~10% of patients with myelodysplastic syndrome (MDS), but are rare in acute myeloid leukaemia (AML). Recent studies have shown that *EZH2* mutations are often associated with *RUNX1* mutations in MDS patients, although its pathological function remains to be addressed. Here we establish an MDS mouse model by transducing a *RUNX1S291fs* mutant into hematopoietic stem cells and subsequently deleting *Ezh2*. Ezh2 loss significantly promotes RUNX1S291fs-induced MDS. Despite their compromised proliferative capacity of *RUNX1S291fs/Ezh2*-null MDS cells, MDS bone marrow impairs normal hematopoietic cells via selectively activating inflammatory cytokine responses, thereby allowing propagation of MDS clones. In contrast, loss of Ezh2 prevents the transformation of AML via PRC1-mediated repression of *Hoxa9*. These findings provide a comprehensive picture of how Ezh2 loss collaborates with *RUNX1* mutants in the pathogenesis of MDS in both cell autonomous and non-autonomous manners.

[1] Department of Cellular and Molecular Medicine, Graduate School of Medicine, Chiba University, 1-8-1 Inohana, Chuo-ku, Chiba 260-8670, Japan. [2] JST, CREST, 7 Gobancho, Chiyoda-ku, Tokyo 102-0076, Japan. [3] Department of Hematology and Oncology, Research Institute for Radiation Biology and Medicine, Hiroshima University, 1-2-3 Kasumi, Minami-ku, Hiroshima 734-8553, Japan. [4] Division of Molecular Oncology, Research Institute for Radiation Biology and Medicine, Hiroshima University, 1-2-3 Kasumi, Minami-ku, Hiroshima 734-8553, Japan. [5] Division of Radiation Information Registry, Research Institute for Radiation Biology and Medicine, Hiroshima University, 1-2-3 Kasumi, Minami-ku, Hiroshima 734-8553, Japan. [6] Department of Hematology, Chiba University Hospital, 1-8-1 Inohana, Chuo-ku, Chiba 260-8670, Japan. [7] Division of Pathology, Cincinnati Children's Hospital Medical Center, 3333 Burnet Avenue, Cincinnati, Ohio 45229-3026, USA. [8] Division of Experimental Hematology and Cancer Biology, Cincinnati Children's Hospital Medical Center, 3333 Burnet Avenue, Cincinnati, Ohio 45229-3026, USA. [9] Department of Allergy and Clinical Immunology, Graduate School of Medicine, Chiba University, 1-8-1 Inohana, Chuo-ku, Chiba 260-8670, Japan. [10] Laboratory for Lymphocyte Development, RIKEN Center for Integrative Medical Sciences, 1-7-22 Suehiro-cho, Tsurumi-ku, Yokohama, Kanagawa 230-0045, Japan. [11] Division of Cellular Therapy and Division of Stem Cell Signaling, Institute of Medical Science, University of Tokyo, 4-6-1 Shirokanedai, Minato, Tokyo 108-8639, Japan. † Present address: Department of Hematology, Juntendo University School of Medicine, 2-1-1 Hongo, Bunkyo-ku, Tokyo 113-8421, Japan. Correspondence and requests for materials should be addressed to G.S. (email: gorosashida@faculty.chiba-u.jp) or to A.I. (email: aiwama@faculty.chiba-u.jp).

© 2014 Macmillan Publishers Limited. All rights reserved.

Recent genome sequencing studies have identified various mutations of epigenetic regulators in patients with myeloid malignancies such as myelodysplastic syndrome (MDS), myeloproliferative neoplasm (MPN) and acute myeloid leukaemia (AML)[1–3]. Epigenetic alterations are involved in the establishment of gene expression profiles associated with cancers, and the accumulation of genetic and epigenetic alterations promote tumorigenesis[4,5].

Among epigenetic regulators, polycomb-group (PcG) proteins have been implicated in many types of cancer. PcG proteins compose the polycomb repressive complexes 1 and 2 (PRC1 and PRC2), and function to repress the transcription of genes through monoubiquitination at H2AK119 (H2AK119ub1) and trimethylation at H3K27 (H3K27me3), respectively[6,7]. In the canonical pathway, PRC2 initiates gene silencing by catalysing H3K27me3 modification. PRC1 is then recruited to the target regions by binding to H3K27me3 through the CBX component of PRC1 (ref. 8), and then catalyses the monoubiquitination of H2AK119 to maintain gene silencing[9]. However, recent findings have shown that PRC1 can be recruited to target genes independently of H3K27me3 (refs 10,11). For example, the RUNX1 transcription factor has been shown to physically bind to Bmi1, a component of PRC1, and to recruit PRC1 in a PRC2-independent manner during the differentiation of megakaryocytes[12]. Since overexpression or gain-of-function mutations of *EZH2*, a catalytic component of PRC2, are often found in carcinomas and lymphomas[2,13], PcG genes have traditionally been characterized as oncogenes[5]. Specifically, overexpression of *Ezh2* has been shown to lead to MPN[14]. We also reported that disease caused by MLL-AF9 requires Ezh2 for progression into AML in a mouse model[15]. These findings highlight the oncogenic function of EZH2 and are consistent with the findings that loss-of-function mutations of *EZH2* are rare in *de novo* AML patients[2,16]. In contrast, ~10% of MDS patients harbour loss-of-function mutations in *EZH2* (refs 16,17), excluding −7/7q− chromosome anomalies, which involves *EZH2* located at 7q36. *EZH2* mutations in MDS patients are associated with significantly worse prognosis, which is not due to AML transformation[1,18]. In addition, MDS patients without −7/7q− chromosome anomalies have reduced expression of *EZH2* in $CD34^+$ cells[19], suggesting that EZH2 functions as a tumour suppressor in MDS. Indeed, we have recently shown that concurrent depletion of *Ezh2* and *Tet2* markedly accelerates the development of MDS and MDS/MPN in mice[20]. However, much remains unknown how *EZH2* loss due to −7/7q− anomalies and loss-of-function mutations of *EZH2* promotes the development of MDS.

RUNX1 (also known as *AML1/CBFA2*), a transcription factor critical for hematopoiesis, is frequently mutated (10–20%) in MDS patients and its mutations are significantly associated with −7/7q− chromosome anomalies[21,22]. Recent studies have demonstrated that *RUNX1* mutations are one of several alterations significantly associated with *EZH2* mutations in MDS patients and that both mutations independently predict poor prognosis[1,18,23]. *RUNX1S291fs* mutant retains a DNA binding domain but lacks a transactivation domain in the carboxy terminus[22]. It has been demonstrated that transduction of *RUNX1S291fs* into bone marrow (BM) progenitor cells is sufficient to induce MDS and AML following MDS (MDS/AML) *in vivo*, although it takes a long latency[24].

Given these findings, we set about to understand the molecular mechanism underlying the pathogenesis of MDS. We established a novel MDS mouse model utilizing *Ezh2*-dificient hematopoietic stem cells (HSCs) and the *RUNX1S291fs* mutant. In this study, we found that Ezh2 loss significantly promoted the transformation of HSCs expressing the *RUNX1S291fs* mutant into MDS cells *in vivo*. Of note, *RUNX1S291fs/Ezh2*-null hematopoietic stem/progenitor cells (HSPCs) did not activate the expression of potent leukaemic oncogenes such as *Hoxa9* and *Mecom/Evi1* and showed compromised proliferative capacity, consistent with the impaired proliferative capacity of human MDS HSPCs[25]. We also found *HOXA9* expression to be closely repressed in $CD34^+$ HSPCs from the early stage MDS patients. While deregulation of HSC function is an important step for the development of myeloid malignancies[26], recent studies indicate that BM microenvironment is another critical factor for the development of myeloid malignancies including MDS[27,28]. Chronic myeloid leukaemia (CML) cells also affect the function of BM microenvironment to impair normal hematopoiesis and support CML stem cell function[29,30]. Here, despite the compromised proliferative capacity, *RUNX1S291fs/Ezh2*-null MDS cells outcompete residing wild-type (WT) cells in the MDS BM by activating inflammatory cytokine responses, including the interleukin-6 (IL-6) pathway, which have been shown to impair normal HSCs *in vivo*. Thus, the MDS BM environment negatively impacts normal HSCs, but not the MDS cells, thereby allowing propagation of MDS clones. Finally, we demonstrate that Ezh2 loss is incompatible with the leukaemic transformation of MDS clones partly due to the inactivation of *Hoxa9* on loss of Ezh2.

Results

Ezh2 loss promotes RUNX1 mutant-induced MDS. Given that *RUNX1* mutations are identified in ~30% of MDS patients harbouring *EZH2* loss-of-function mutations[1,18,23], we examined how *Ezh2* loss and *RUNX1* mutants collaborate in the development of MDS *in vivo*. To do so, we transduced a *RUNX1S291fs-IRES-GFP* or a control *empty-IRES-GFP* retroviral construct into either *Cre-ERT;Ezh2*$^{wt/wt}$ or *Cre-ERT;Ezh2*$^{flox/flox}$ ($CD45.2^+$) $CD34^-$ $Lin^-Sca1^-c\text{-}Kit^+$ (LSK) HSCs (Fig. 1a). The transduced cells were transplanted into lethally irradiated $CD45.1^+$-recipient mice together with radioprotective $CD45.1^+$ BM cells (Fig. 1a). The $CD45.2^+GFP^+$-transduced cells successfully engrafted and established significant levels of chimerism in the peripheral blood (PB) at 1 month post transplantation (Supplementary Fig. 1), and expressed the RUNX1S291fs protein (Fig. 1b). We then proceeded to activate Cre-ERT recombinase at 6 weeks post transplantation by intraperitoneal injection of tamoxifen (Fig. 1a). We hereafter refer to the recipient mice reconstituted with *Empty/Ezh2*$^{wt/wt}$, *Empty/Ezh2*$^{\Delta/\Delta}$, *RUNX1S291fs/Ezh2*$^{wt/wt}$ and *RUNX1S291fs/Ezh2*$^{\Delta/\Delta}$-transduced HSCs as WT, Ezh2$^{\Delta/\Delta}$, Rx291 and Rx291/Ezh2$^{\Delta/\Delta}$ mice, respectively (Fig. 1a). We confirmed successful deletions of *Ezh2* (Supplementary Fig. 2), and markedly reduced the levels of H3K27me3 in $CD45.2^+GFP^+Lin^-c\text{-}Kit^+$ BM cells isolated from Ezh2$^{\Delta/\Delta}$ and Rx291/Ezh2$^{\Delta/\Delta}$ mice (Fig. 1b). Although levels of *RUNX1S291fs* transcripts were comparable between *Rx291* and *Rx291/Ezh2*$^{\Delta/\Delta}$ cells (Supplementary Fig. 3), level of RUNX1S291fs protein was much higher in *Rx291/Ezh2*$^{\Delta/\Delta}$ cells (Fig. 1b), suggesting that Ezh2 loss somehow impacts the levels of RUNX1S291fs protein post transcriptionally.

We first examined whether Ezh2 loss contributes to the development of MDS in recipient mice. While WT mice ($n=9$) and Ezh2$^{\Delta/\Delta}$ mice ($n=9$) did not develop lethal haematological malignancies within 10 months post transplantation, Rx291 and Rx291/Ezh2$^{\Delta/\Delta}$ mice developed MDS. Rx291/Ezh2$^{\Delta/\Delta}$ mice showed a significantly shorter median survival than Rx291 mice did (262 days versus undetermined, $P=0.038$) (Fig. 1c), indicating that Ezh2 loss facilitates disease progression. Although Rx291/Ezh2$^{\Delta/\Delta}$ mice did not show any significant changes in the peripheral complete blood counts until 3 months post transplantation, they started to show reduced haemoglobin levels and increased mean corpuscular volume compared with WT mice at

© 2014 Macmillan Publishers Limited. All rights reserved.

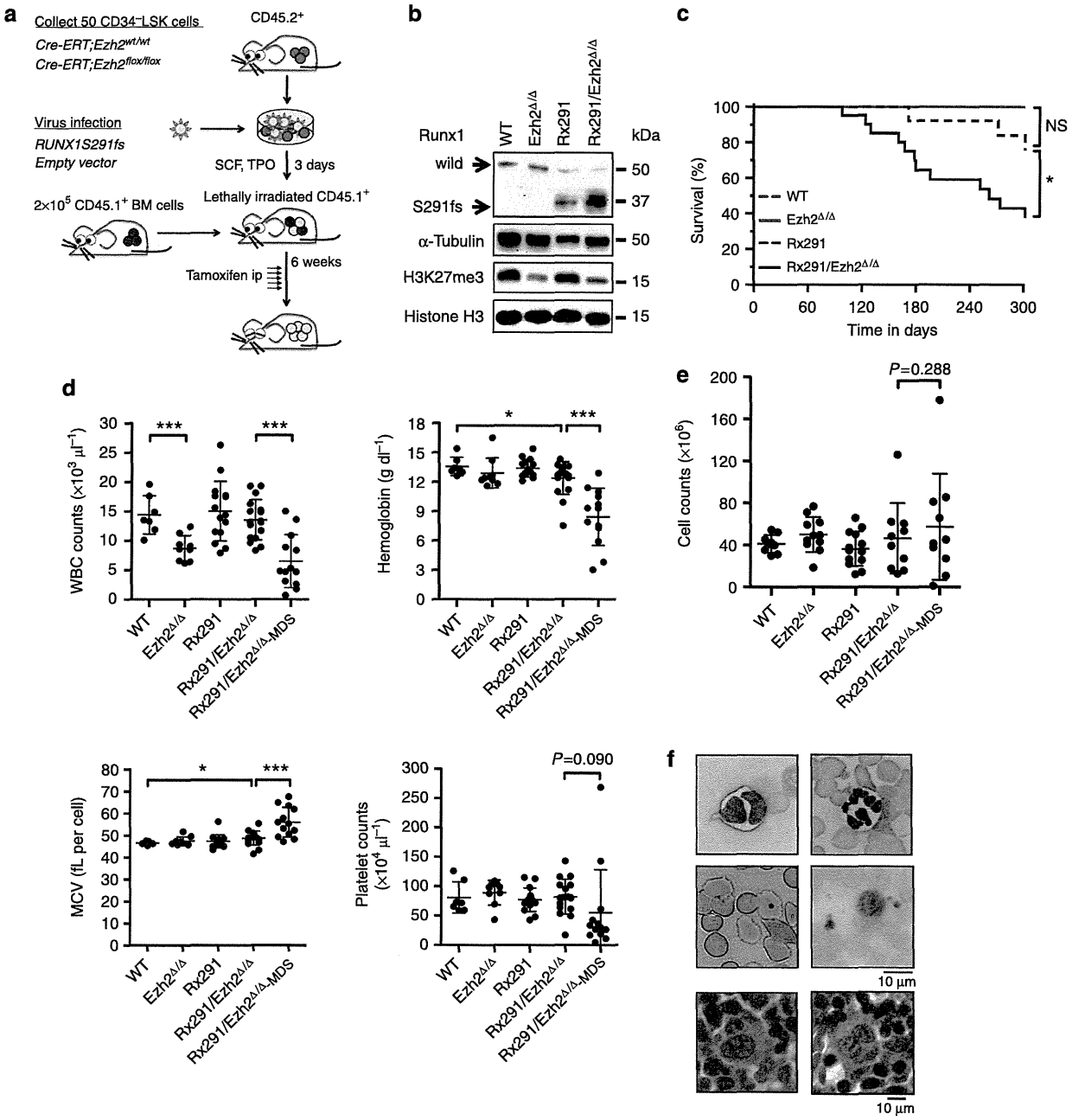

Figure 1 | Ezh2 loss promotes formation of RUNX1S291fs mutant-induced MDS. (**a**) Experimental scheme of our model mouse utilizing *RUNX1S291fs* mutant and *Ezh2* conditional knockout HSCs. (**b**) Successful transductions of RUNX1S291fs protein and levels of H3K27me3 in Lin$^-$c-Kit$^+$ cells detected by western blotting. α-Tubulin and histone H3 were detected as loading controls. (**c**) Significantly shorter median survival of Rx291/Ezh2$^{\Delta/\Delta}$ mice ($n=21$) compared with Rx291 mice ($n=18$) (262 days versus undetermined, $P=0.038$ by Log-rank test). (**d**) Complete blood cell counts of WT ($n=7$), Ezh2$^{\Delta/\Delta}$($n=9$), Rx291 ($n=15$) and Rx291/Ezh2$^{\Delta/\Delta}$ ($n=17$) mice at 4 months post transplantation (pre-MDS stage) and moribund Rx291/Ezh2$^{\Delta/\Delta}$-MDS mice ($n=13$). Rx291/Ezh2$^{\Delta/\Delta}$ mice showed reduced hemoglobin levels and increased mean corpuscular volume (MCV) compared with WT mice (12.4 ± 1.7 versus 13.6 ± 0.9, $P=0.047$ and 48.7 ± 3.2 versus 46.5 ± 0.7, $P=0.048$ by Student's *t*-test, respectively). Moribund Rx291/Ezh2$^{\Delta/\Delta}$-MDS mice showed significant leukopenia and macrocytic anaemia compared with Rx291/Ezh2$^{\Delta/\Delta}$ mice at 4 months post transplantation (pre-MDS stage). Scale bars and asterisks show mean ± s.d., $^*P<0.05$, $^{**}P<0.01$, and $^{***}P<0.001$ by Student's *t*-test. (**e**) BM cell counts (from bilateral femurs and tibiae) in WT, Ezh2$^{\Delta/\Delta}$, Rx291 and Rx291/Ezh2$^{\Delta/\Delta}$ mice at 4 months post transplantation (pre-MDS stage) and moribund Rx291/Ezh2$^{\Delta/\Delta}$-MDS mice. Comparable cell counts were seen in Rx291/Ezh2$^{\Delta/\Delta}$ ($n=10$) and Rx291/Ezh2$^{\Delta/\Delta}$-MDS mice ($n=10$). Scale bars show mean ± s.d. *P*-value was determined by Student's *t*-test. (**f**) Appearance of dysplastic blood cells in Rx291/Ezh2$^{\Delta/\Delta}$-MDS mice observed by May-Grüenwald Giemsa staining. Pseudo-Pelger-Huët cell (PB), hypersegmented neutrophil (PB), a giant platelet (PB), hypolobated megakaryocytes (BM) and nucleated red blood cells (PB) are depicted (clockwise from the upper left picture). Scale bars, 10 μm. ip, intraperitoneal.

4 months post transplantation (Fig. 1d). Ezh2$^{\Delta/\Delta}$ mice showed a significant leukopenia, in part due to impaired lymphopoiesis as previously reported[31,32]. While only 2 out of 18 Rx291 mice developed MDS within 10 months post transplantation, 13 out of 21 Rx291/Ezh2$^{\Delta/\Delta}$ mice developed MDS including one MDS/myeloid leukaemia (MDS/ML) showing very slow disease

© 2014 Macmillan Publishers Limited. All rights reserved.

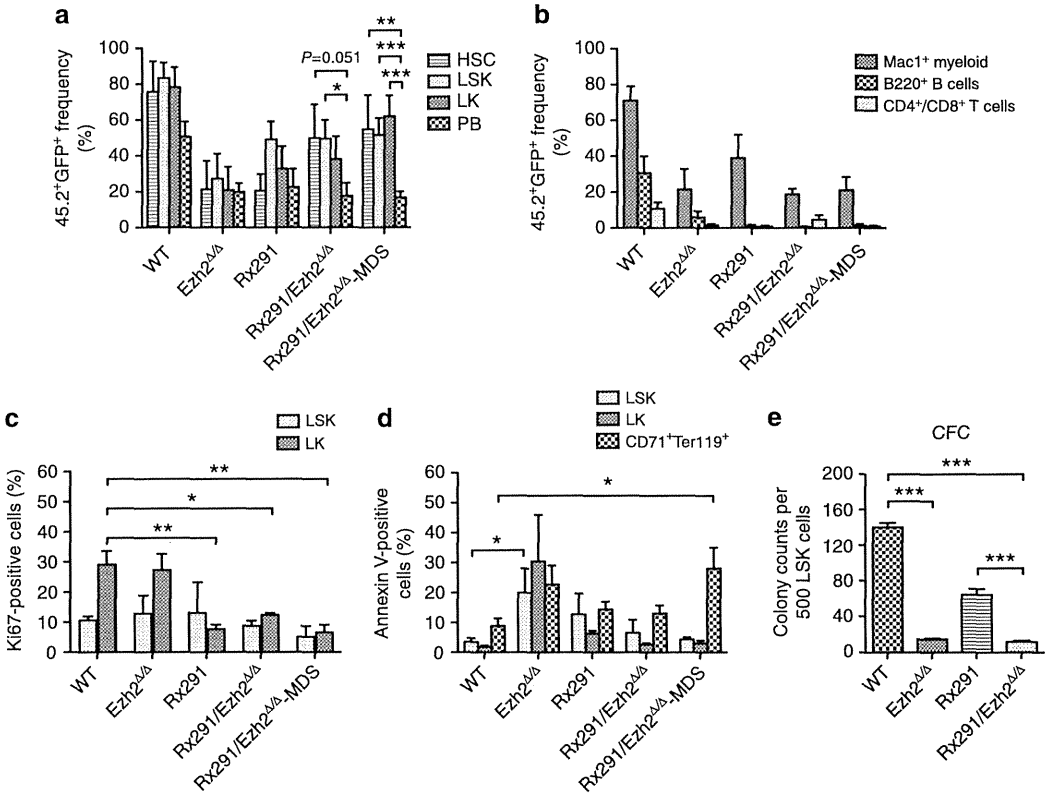

Figure 2 | Ezh2 loss confers a competitive disadvantage to RUNX1S291fs-expressing HSPCs. (**a**) Chimerism of CD45.2$^+$GFP$^+$ cells in HSCs, LSK cells and LK cells in the BM and PB cells in WT, Ezh2$^{\Delta/\Delta}$, Rx291 and Rx291/Ezh2$^{\Delta/\Delta}$ mice at 4 months post transplantation (pre-MDS stage) ($n=4$–6) and moribund Rx291/Ezh2$^{\Delta/\Delta}$-MDS mice ($n=12$). Scale bars and asterisks show mean ± s.d. and $^*P<0.05$, $^{**}P<0.01$ and $^{***}P<0.001$ by Student's *t*-test. (**b**) Chimerism of CD45.2$^+$GFP$^+$ of Mac1$^+$ myeloid cells, B220$^+$ B cells and CD4$^+$/CD8$^+$ T cells in the PB analysed in **a**. Scale bars show mean ± s.d. (**c**) Proliferative capacity examined with Ki67 in (CD45.2$^+$GFP$^+$) LSK and LK cells in WT, Ezh2$^{\Delta/\Delta}$, Rx291 and Rx291/Ezh2$^{\Delta/\Delta}$ mice at 4 months post transplantation ($n=3$–5) and moribund Rx291/Ezh2$^{\Delta/\Delta}$-MDS mice ($n=3$). Scale bars and asterisks show mean ± s.e.m., $^*P<0.05$ and $^{**}P<0.01$ by Student's *t*-test. (**d**) Enhanced apoptosis in CD71$^+$Ter119$^+$ *Rx291/Ezh2*$^{\Delta/\Delta}$-MDS erythroblasts but not in MDS LSK/LK stem and progenitor cells in WT, Ezh2$^{\Delta/\Delta}$, Rx291 and Rx291/Ezh2$^{\Delta/\Delta}$ mice at 4 months post transplantation ($n=3$–6) and moribund Rx291/Ezh2$^{\Delta/\Delta}$-MDS mice ($n=4$). Scale bars and asterisks show mean ± s.e.m. and $^*P<0.05$ by Student's *t*-test. (**e**) Clonogenic capacity of 500 (CD45.2$^+$GFP$^+$) LSK cells isolated from WT, Ezh2$^{\Delta/\Delta}$, Rx291 and Rx291/Ezh2$^{\Delta/\Delta}$ mice at 4 months post transplantation ($n=3$). Scale bars and asterisk show mean ± s.e.m. and $^{***}P<0.001$ by Student's *t*-test.

progression that did not match the criteria of 'acute' leukaemia in the Bethesda proposal (Fig. 1c and Supplementary Table 1)[33]. Moribund Rx291/Ezh2$^{\Delta/\Delta}$ mice with MDS including MDS/ML (Rx291/Ezh2$^{\Delta/\Delta}$-MDS mice) showed significant leukopenia and macrocytic anaemia (anaemia with increased mean corpuscular volume) compared with Rx291/Ezh2$^{\Delta/\Delta}$ mice at pre-MDS stage (Fig. 1d). BM cellularity was variable among Rx291/Ezh2$^{\Delta/\Delta}$-MDS mice, implying heterogeneous disease status (Fig. 1e). Rx291/Ezh2$^{\Delta/\Delta}$-MDS mice also showed dysplastic cells characteristic of human MDS such as pseudo-Pelger–Huët cells, hypersegmented neutrophils, nucleated red blood cells, giant platelets and hypolobated megakaryocytes (Fig. 1f)[34]. Thus, our model mice present with leukopenia, anaemia and multilineage dysplasia, phenotypically recapitulating human MDS. In addition, we also confirmed that Ezh2 loss significantly promotes the development of MDS induced by *RUNX1D171N*, another *RUNX1* mutant defective in DNA binding, although *RUNX1D171N*-mutant cells exhibited a relatively long latency (D171N/Ezh2$^{\Delta/\Delta}$ ($n=5$) versus D171N/Ezh2$^{wt/wt}$ ($n=7$); 353 days versus undetermined, $P=0.0133$ by Log-rank test). These findings indicate that Ezh2 can function as a tumour suppressor in MDS, especially in the presence of RUNX1 mutants.

Ezh2 loss provokes ineffective hematopoiesis. MDS patients show ineffective hematopoiesis characterized by impaired differentiation and enhanced apoptosis of BM cells that leads to cytopenia[35]. To evaluate hematopoiesis in Rx291/Ezh2$^{\Delta/\Delta}$-MDS mice, we first examined chimerism of CD45.2$^+$GFP$^+$ cells in HSCs (CD34$^-$LSK), HSPCs (LSK) and Lin$^-$c-Kit$^+$Sca1$^-$ (LK) myeloid progenitor cells in the BM and myeloid cells and lymphoid cells in the PB. While Ezh2$^{\Delta/\Delta}$ and Rx291 mice showed comparable chimerism of CD45.2$^+$GFP$^+$ mutant cells in both BM and PB, both Rx291/Ezh2$^{\Delta/\Delta}$ (at pre-MDS stage) and Rx291/Ezh2$^{\Delta/\Delta}$-MDS (at terminal stage) mice showed higher chimerism in BM HSCs and HSPCs, but contradictory lower chimerism in PB (Fig. 2a), due to impaired production of Mac1$^+$ myeloid cells, CD4$^+$/CD8$^+$ T cells and B220$^+$ B cells (Fig. 2b). These findings indicate that on deletion of *Ezh2*, *RUNX1S291fs*-expressing HSCs acquire a competitive disadvantage in terms of their ability to generate PB cells.

We then examined proliferative capacity of stem/myeloid progenitor cells by staining with Ki67, a marker for cellular proliferation. Transduction of *RUNX1S291fs* appeared to reduce Ki67$^+$ frequencies in LK myeloid progenitor cells and in LSK cells, and this trend was even more evident in LK cells in Rx291/Ezh2$^{\Delta/\Delta}$-MDS mice (Fig. 2c). Thus, the proliferative capacity of *Rx291/Ezh2*$^{\Delta/\Delta}$ cells was attenuated during the development of MDS, especially in myeloid progenitor cells. As Rx291/Ezh2$^{\Delta/\Delta}$-MDS mice also showed anaemia, we next examined the apoptosis of BM cells by Annexin V staining. Ezh2$^{\Delta/\Delta}$ mice showed

© 2014 Macmillan Publishers Limited. All rights reserved.

Table 1 | Frequency of repopulating cells in RUNX1S291fs-induced cells.

	2×10^4 Lin$^-$c-Kit$^+$	2000 Lin$^-$c-Kit$^+$	200 Lin$^-$c-Kit$^+$	Frequency of repopulating cells	95% CI
Rx291	0/6 mice	0/3 mice	0/3 mice	Undetermined	Undetermined
Rx291/Ezh2$^{\Delta/\Delta}$	2/7 mice	0/5 mice	0/6 mice	1/65,089	1/259,626-1/16,318

BM, bone marrow; CI, confidence interval; GFP, green fluorescence protein; MDS, myelodysplastic syndrome; PB, peripheral blood.
Frequency of repopulating cells was determined by transplantation using limiting doses of RUNX1S291fs-expressing (CD45.2$^+$GFP$^+$) Lin$^-$c-Kit$^+$ cells (2×10^4, 2×10^3 and 200) isolated from Rx291 and Rx291/Ezh2$^{\Delta/\Delta}$ mice at pre-MDS stage together with 2×10^5 competitor CD45.1$^+$ BM cells. Mice showing chimerism of CD45.2$^+$GFP$^+$ cells >1% in PB at 4 months post transplantation were considered to be positively repopulated mice.

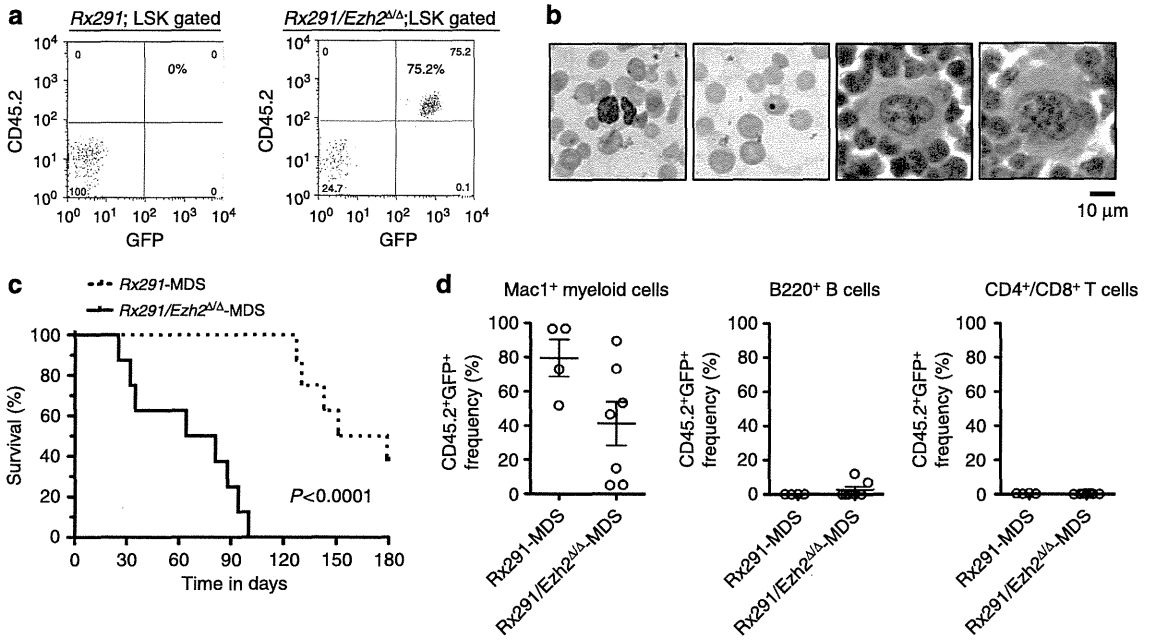

Figure 3 | Ezh2 loss promotes initiation and propagation of RUNX1S291fs-induced MDS. (**a**) Representative flow cytometric profiles of LSK cells in recipient mice infused with 2×10^4 *Rx291* or *Rx291/Ezh2*$^{\Delta/\Delta}$Lin$^-$c-Kit$^+$ cells at 6 months post transplantation. Proportion of CD45.2$^+$GFP$^+$ cells within LSK cells was indicated (%). (**b**) Dysplastic neutrophils, red blood cells and megakaryocytes in the BM of the positively repopulated recipient mice in **a** that developed MDS. Scale bar, 10 μm. (**c**) Significantly shorter median survival of recipients of *Rx291/Ezh2*$^{\Delta/\Delta}$-MDS cells ($n=8$), compared with those of *Rx291*-MDS cells ($n=8$)(72.5 days versus 165 days; $P<0.0001$ by Log-rank test). Lethally irradiated recipient mice were infused with 1×10^6 CD45.2$^+$GFP$^+$ RUNX1S291fs-expressing BM cells isolated from Rx291-MDS mice or Rx291/Ezh2$^{\Delta/\Delta}$-MDS mice together with 2×10^5 competitor CD45.1$^+$ BM cells. (**d**) Chimerism of CD45.2$^+$GFP$^+$ cells in Mac1$^+$ myeloid cells, B220$^+$ B cells and CD4$^+$/CD8$^+$ T cells in the PB in Rx291-MDS ($n=4$) and Rx291/Ezh2$^{\Delta/\Delta}$-MDS recipient mice ($n=7$) at the advanced MDS stage. Scale bars show mean ± s.e.m.

enhanced apoptosis especially in LSK cells (Fig. 2d). Rx291/Ezh2$^{\Delta/\Delta}$-MDS mice showed enhanced apoptosis in (CD45.2$^+$GFP$^+$) CD71$^+$Ter119$^+$ erythroblasts, but not in LK and LSK cells, compared with WT mice (Fig. 2d), implying that RUNX1S291fs mutant suppressed the Ezh2 loss-induced apoptosis in LSK cells. Previous studies have shown that the *in vitro* colony-forming capacity of HSPCs isolated from MDS patients and MDS mouse models is impaired[25,36]. Consistent with these findings, we found that *Rx291/Ezh2*$^{\Delta/\Delta}$ LSK cells generated significantly fewer colonies *in vitro* than WT and *Rx291* LSK cells (Fig. 2e). Taken together, the impaired proliferative capacity of myeloid progenitor cells and enhanced apoptosis in erythroblasts may account for the cytopenia observed in Rx291/Ezh2$^{\Delta/\Delta}$-MDS mice. Thus, our mouse model also recapitulates ineffective hematopoiesis, one of the pathological features of MDS.

Ezh2 loss promotes initiation and propagation of MDS. Since *Rx291/Ezh2*$^{\Delta/\Delta}$HSPCs were capable of potent induction of MDS despite their impaired proliferative capacity and competitive disadvantage in generating PB cells, we examined the repopulating capacity of *Rx291* and *Rx291/Ezh2*$^{\Delta/\Delta}$ cells in detail by employing a limiting dilution transplantation assay utilizing 2×10^4, 2×10^3 and 200 CD45.2$^+$GFP$^+$Lin$^-$c-Kit$^+$ cells isolated from the primary Rx291 and Rx291/Ezh2$^{\Delta/\Delta}$ mice at pre-MDS stage together with 2×10^5 competitor CD45.1$^+$ BM cells. We considered the recipient mice showing chimerism of CD45.2$^+$GFP$^+$ cells >1% in PB at 4 months post transplantation as positively repopulated mice. *Rx291* Lin$^-$c-Kit$^+$ cells did not repopulate any mice in any experiments, whereas *Rx291/Ezh2*$^{\Delta/\Delta}$ Lin$^-$c-Kit$^+$ cells at a dose of 2×10^4 cells positively repopulated two out of seven recipient mice, allowing estimation of the frequency of repopulating cells to be between 1 in 259,626 and 1 in 16,318 Lin$^-$c-Kit$^+$ cells (95% confidence interval)(Table 1). Notably, these *Rx291/Ezh2*$^{\Delta/\Delta}$cells repopulated in the positive mice outcompeted the WT competitor cells in the BM (Fig. 3a), and induced MDS by 6 months post transplantation as indicated by dysplastic neutrophils, nucleated red blood cells, hypolobated megakaryocytes in the BM (Fig. 3b), as well as mild macrocytic anaemia. Thus, loss of *Ezh2* promotes the expansion of MDS-initiating cells in HSPCs expressing *RUNX1S291fs* at the 'pre-MDS phase'.

© 2014 Macmillan Publishers Limited. All rights reserved.

Table 2 | GSEA for Ezh2 targets and AML-related targets.

	$Ezh2^{\Delta/\Delta}$	*Rx291*	*Rx291/*$Ezh2^{\Delta/\Delta}$	*Rx291/*$Ezh2^{\Delta/\Delta}$ -MDS	*Rx291/*$Ezh2^{\Delta/\Delta}$ -MDS/ML
Ezh2 targets	1.37/0.001	1.15/0.118	1.15/0.142	−1.41/0.001	−1.27/0.031
HSCs fingerprints	0.85/0.764	−2.03/0.000	−2.67/0.000	−2.73/0.000	−2.61/0.000
MLL-AF9	−1.62/0.000	−0.91/1.0	1.17/0.671	−1.52/0.009	−1.51/0.009
NUP98-HOXA9	1.20/0.104	−1.32/0.000	−1.85/0.000	−1.94/0.000	−1.97/0.000

AML, acute myeloid leukemia; FDR, false discovery rate; GSEA, gene set enrichment analysis; HSC, hematopoietic stem cell; MDS, myelodysplastic syndrome; ML, myeloid leukemia; NES, normalized enrichment score; WT, wild type.
GSEA for Ezh2 targets, HSC fingerprints, AML-related targets of *MLL-AF9* and *NUP98-HOXA9* in CD45.2$^+$GFP$^+$ LSK cells from $Ezh2^{\Delta/\Delta}$, Rx291 and Rx291/$Ezh2^{\Delta/\Delta}$ mice at 4 months post transplantation (pre-MDS stage) and moribund Rx291/$Ezh2^{\Delta/\Delta}$-MDS and MDS/ML mice, compared with those from WT mice. NES and FDR *q*-value are shown in each cell. Red and blue colours represent positive (upregulated in the given genotype relative to WT) and negative (downregulated in WT relative to the given genotype) enrichment, respectively. Concentrated colours show that the nominal *P*-value is less than 0.05 and FDR is less than 0.05, which suggest meaningful enrichment for the given gene sets. Pale colours show borderline enrichment with FDR *q*-value between 0.05 and 0.25. The white colour cells do not meet these criteria.

Since both Rx291 and Rx291/$Ezh2^{\Delta/\Delta}$ mice developed MDS albeit with different latencies (Fig. 1c), we next investigated whether *RUNX1S291fs*-induced MDS cells could propagate in secondary recipients in the absence of Ezh2. We transplanted 1×10^6 CD45.2$^+$GFP$^+$ RUNX1S291fs-expressing BM cells isolated from Rx291-MDS and Rx291/$Ezh2^{\Delta/\Delta}$-MDS mice independently into lethally irradiated CD45.1$^+$ recipient mice together with 2×10^5 CD45.1$^+$ BM cells. We found that all secondary recipients infused with *Rx291/*$Ezh2^{\Delta/\Delta}$-MDS cells died from MDS within 100 days, whereas those with *Rx291*-MDS cells took much longer to develop lethal MDS (median survival, 72.5 days versus 165 days; $P<0.0001$) (Fig. 3c). Furthermore, production of peripheral myeloid cells by *Rx291/*$Ezh2^{\Delta/\Delta}$-MDS cells appeared to be less efficient compared with *Rx291*-MDS cells at the advanced MDS stage (Fig. 3d), again suggesting ineffective hematopoiesis by *Rx291/*$Ezh2^{\Delta/\Delta}$-MDS cells. These findings indicate that *Ezh2* loss promotes both initiation and propagation of *RUNX1S291fs*-induced MDS.

Ezh2 target genes were repressed in *Ezh2*-null MDS HSPCs. To understand how Ezh2 loss promotes RUNX1S291fs-induced MDS, we began to investigate gene expression profiles in CD45.2$^+$GFP$^+$LSK cells isolated from WT, $Ezh2^{\Delta/\Delta}$, Rx291, Rx291/$Ezh2^{\Delta/\Delta}$ (at 4 months post transplantation), and two Rx291/$Ezh2^{\Delta/\Delta}$-MDS mice (MDS and MDS/ML). Since Ezh2 functions to repress transcription via H3K27me3 modification, its absence is supposed to activate transcription of its target genes. As expected, gene set enrichment analysis (GSEA) revealed that $Ezh2^{\Delta/\Delta}$ LSK cells significantly de-repressed canonical Ezh2 target genes (Table 2 and Supplementary Fig. 4), defined in murine ES cells (GSE15388)[37]. However, Ezh2 targets were negatively enriched in both *Rx291/*$Ezh2^{\Delta/\Delta}$-MDS and MDS/ML LSK cells, compared with WT LSK cells (Table 2). Repression of Ezh2 target genes was also evident when we compared *Rx291/*$Ezh2^{\Delta/\Delta}$-MDS LSK cells to *Rx291/*$Ezh2^{\Delta/\Delta}$LSK cells at the pre-MDS phase (Fig. 4a), indicating that Ezh2 targets underwent transcriptional repression during the development of MDS despite the absence of Ezh2. This finding is similar to our previous observations on MDS developed in $Tet2^{KD/KD}Ezh2^{\Delta/\Delta}$ mice compound for *Tet2* hypomorphic gene trap ($Tet2^{KD/KD}$) and conditional deletion of *Ezh2*, where repression of Ezh2 target genes was attributed to the compensatory function of Ezh1, another catalytic component of PRC2 (ref. 20).

We next examined the expression of 'HSC fingerprint genes', a gene set specific to HSCs defined by extensive microarray analyses[38]. *RUNX1S291fs* repressed expression of 'HSC fingerprint genes' and this trend was more evident in *Rx291/*$Ezh2^{\Delta/\Delta}$and *Rx291/*$Ezh2^{\Delta/\Delta}$-MDS LSK cells (Table 2 and Supplementary Fig. 4). RT–PCR analysis confirmed down-regulation of 'HSC fingerprint genes' such as *Mecom/Evi1* (Fig. 4b), which is a well-known oncogene that plays a critical role for both HSCs and AML[39]. Of note, expression of *Mecom/Evi1* became further repressed in *Rx291/*$Ezh2^{\Delta/\Delta}$-MDS LSK cells, compared with *Rx291/*$Ezh2^{\Delta/\Delta}$ LSK cells (Fig. 4b), suggesting that some epigenetic events took place during the disease progression at the *Mecom/Evi1* region.

Promoter DNA hypermethylation is one of the most well-known epigenetic events that propagates during tumour development[40]. We postulated that promoter DNA hypermethylation might also be involved in the transcriptional repression of Ezh2 targets and 'HSC fingerprint genes' in the absence of Ezh2. To evaluate promoter DNA hypermethylation in LSK cells, we performed reduced representation bisulphite sequencing (RRBS). Compared with WT (CD45.2$^+$GFP$^+$) LSK cells, we found 232, 512 and 204 hypermethylated promoters in *Rx291*, *Rx291/*$Ezh2^{\Delta/\Delta}$ and *Rx291/*$Ezh2^{\Delta/\Delta}$-MDS (CD45.2$^+$GFP$^+$) LSK cells, respectively (annotated gene lists are shown in Supplementary Data 1). Notably, the promoter regions of *Mecom/Evi1* acquired DNA hypermethylation in *Rx291/*$Ezh2^{\Delta/\Delta}$ and *Rx291/*$Ezh2^{\Delta/\Delta}$-MDS LSK cells, but not in *Rx291* LSK cells, (Fig. 4c). This hypermethylation was coincided loss of H3K27me3 at the promoter on deletion of *Ezh2* (Fig. 4d). These findings imply that *Mecom/Evi1* is a direct target of Ezh2 in this context. We next examined the correlation between canonical Ezh2 targets in ES cells and genes that underwent DNA hypermethylation identified in this study. Some DNA hypermethylated genes overlapped with the canonical Ezh2 targets in *Rx291/*$Ezh2^{\Delta/\Delta}$ LSK cells (16 out of 374 genes, $P=0.886$) and *Rx291/*$Ezh2^{\Delta/\Delta}$-MDS LSK cells (16 out of 168 genes, $P=0.0284$), but not in *Rx291* LSK cells (Fig. 4e), and appeared to be developmental regulators of hematopoietic and non-hematopoietic lineages (for example, *Mecom/Evi1*, *Pdx1* and *Hand1*) (Supplementary Table 2), suggesting that aberrant promoter DNA hypermethylation is an alternative epigenetic mechanism that represses Ezh2 targets in the absence of Ezh2.

***RUNX1S291fs/Ezh2*-null cells compromise normal HSPCs function.** Although *Rx291/*$Ezh2^{\Delta/\Delta}$ HSPCs did not show enhanced proliferative capacity, *Rx291/*$Ezh2^{\Delta/\Delta}$ cells were able to induce MDS at a lower dose compared with *Rx291* cells.

© 2014 Macmillan Publishers Limited. All rights reserved.

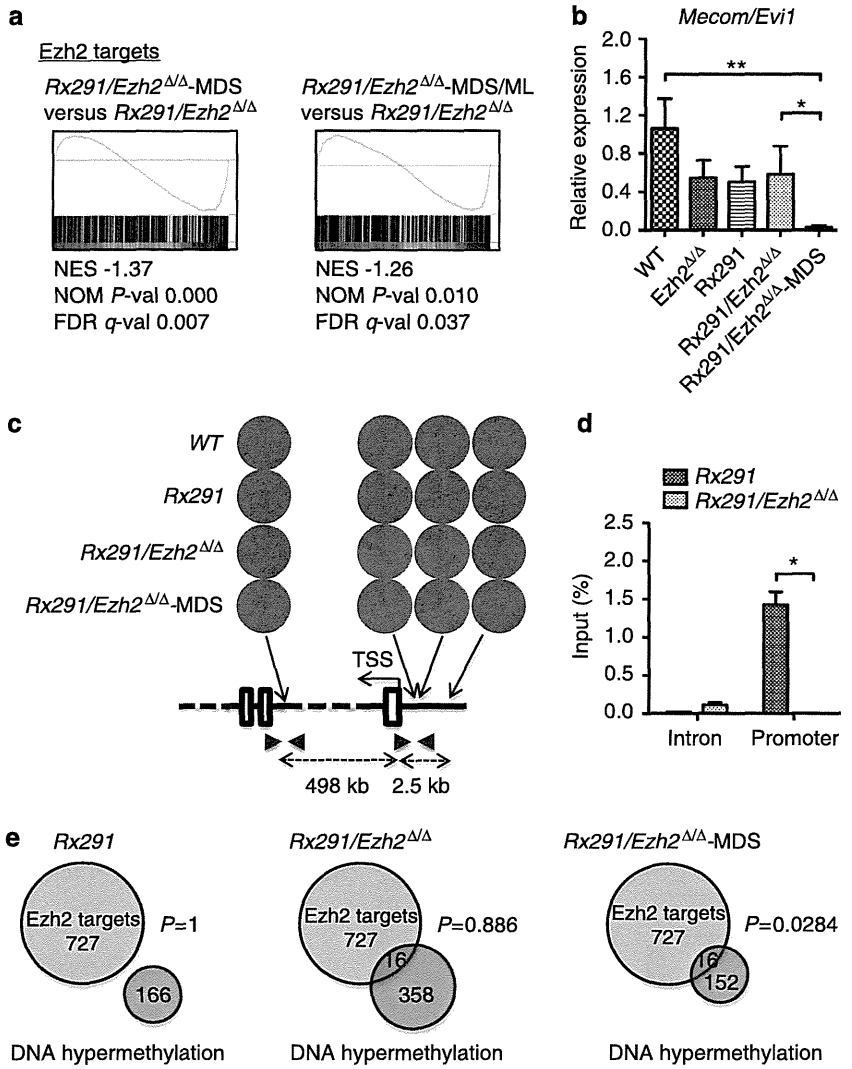

Figure 4 | *RUNX1S291fs/Ezh2*-null MDS HSPCs represses expression of Ezh2 target genes. (**a**) Gene set enrichment plots for the canonical Ezh2 target gene set comparing *Rx291/Ezh2*$^{\Delta/\Delta}$-MDS (left panel) and *Rx291/Ezh2*$^{\Delta/\Delta}$-MDS/ML (right panel) LSK cells with *Rx291/Ezh2*$^{\Delta/\Delta}$ LSK cells at pre-MDS stage. (**b**) Quantitative RT-PCR analysis of the expression of *Mecom/Evi1* in CD45.2$^+$GFP$^+$ LSK cells from in WT, Ezh2$^{\Delta/\Delta}$, Rx291 and Rx291/Ezh2$^{\Delta/\Delta}$ mice at 4 months post transplantation (pre-MDS stage) and moribund Rx291/Ezh2$^{\Delta/\Delta}$-MDS mice ($n=4$–5). Scale bars and asterisks show mean ± s.e.m., $^*P<0.05$ and $^{**}P<0.01$ by Mann-Whitney *U*-test. (**c**) DNA methylation status at promoter and intron regions of *Mecom/Evi1* detected by RRBS in LSK cells from WT, Rx291 and Rx291/Ezh2$^{\Delta/\Delta}$ mice at 4 months post transplantation (pre-MDS stage) and from moribund Rx291/Ezh2$^{\Delta/\Delta}$-MDS mouse. The proportion of methylated (in blue) and non-methylated (in red) cytosines at mm9 position chr3:29911333 (downstream intron), chr3:30409294 and 30409295 (promoter) and chr3:30407526 (upstream) are depicted in circles. Blue arrowheads indicate regions amplified by ChIP-QPCR in **d**. (**d**) The levels of H3K27me3 at the promoter and intron regions of *Mecom/Evi1* in *Rx291* and *Rx291/Ezh2*$^{\Delta/\Delta}$ LSK cells as detected by ChIP-QPCR. The relative amounts of immunoprecipitated DNA are depicted as a percentage of input DNA. Scale bars and asterisks show mean ± s.e.m. ($n=4$), and $^*P<0.05$ by Mann-Whitney *U*-test. (**e**) Venn diagrams of overlaps between canonical Ezh2 target genes and DNA hypermethylated genes in *Rx291*, *Rx291/Ezh2*$^{\Delta/\Delta}$ or *Rx291/Ezh2*$^{\Delta/\Delta}$-MDS LSK cells. Total number of genes was 13146. *P*-value of intersection was determined by using *R* code.

However, the mechanism by which the *Rx291/Ezh2*$^{\Delta/\Delta}$ cells outcompeted WT cells was unclear. Given that BM environment is critical for the development of myeloid malignancies[27,28], we postulated that CD45.1$^+$ WT cells in Rx291/Ezh2$^{\Delta/\Delta}$ mice might be depleted via indirect mechanisms associated with MDS. We did not see obvious differences in the frequencies of phenotypic LSK HSPCs in CD45.1$^+$ cells between Rx291 and Rx291/Ezh2$^{\Delta/\Delta}$ mice ($n=4$; mean ± s.d. 0.0495 ± 0.0668% versus 0.0661 ± 0.0449%; $P=0.694$ by Student's *t*-test). However, colony-forming cells were significantly reduced in CD45.1$^+$ WT LSK cells isolated from Rx291/Ezh2$^{\Delta/\Delta}$ mice, compared with those from Rx291 mice and the primary WT LSK cells (Supplementary Fig. 5). To assess the repopulating capacity of CD45.1$^+$ WT HSPCs *in vivo*, 2×10^5 CD45.1$^+$ WT BM cells isolated from Rx291 mice or Rx291/Ezh2$^{\Delta/\Delta}$ mice were transplanted with an equal number of 8-week-old CD45.2$^+$ competitor BM cells into lethally irradiated CD45.2$^+$-recipient mice (Fig. 5a). CD45.1$^+$ cells from Rx291/Ezh2$^{\Delta/\Delta}$ mice scarcely contributed to LSK cells in BM and mature hematopoietic cells in PB at 4 months post competitive transplantation, whereas CD45.1$^+$ cells from Rx291 mice reconstituted hematopoiesis efficiently (Fig. 5b). These findings indicate that the function of WT HSPCs in Rx291/Ezh2$^{\Delta/\Delta}$ mice is markedly impaired. To understand the underlying mechanism, we examined gene expression profiles of CD45.1$^+$ LSK cells isolated from Rx291 and Rx291/Ezh2$^{\Delta/\Delta}$ mice. Recent studies indicated that inflammatory cytokines are critical factors to regulate normal HSCs under both homeostatic and stress conditions such as

© 2014 Macmillan Publishers Limited. All rights reserved.

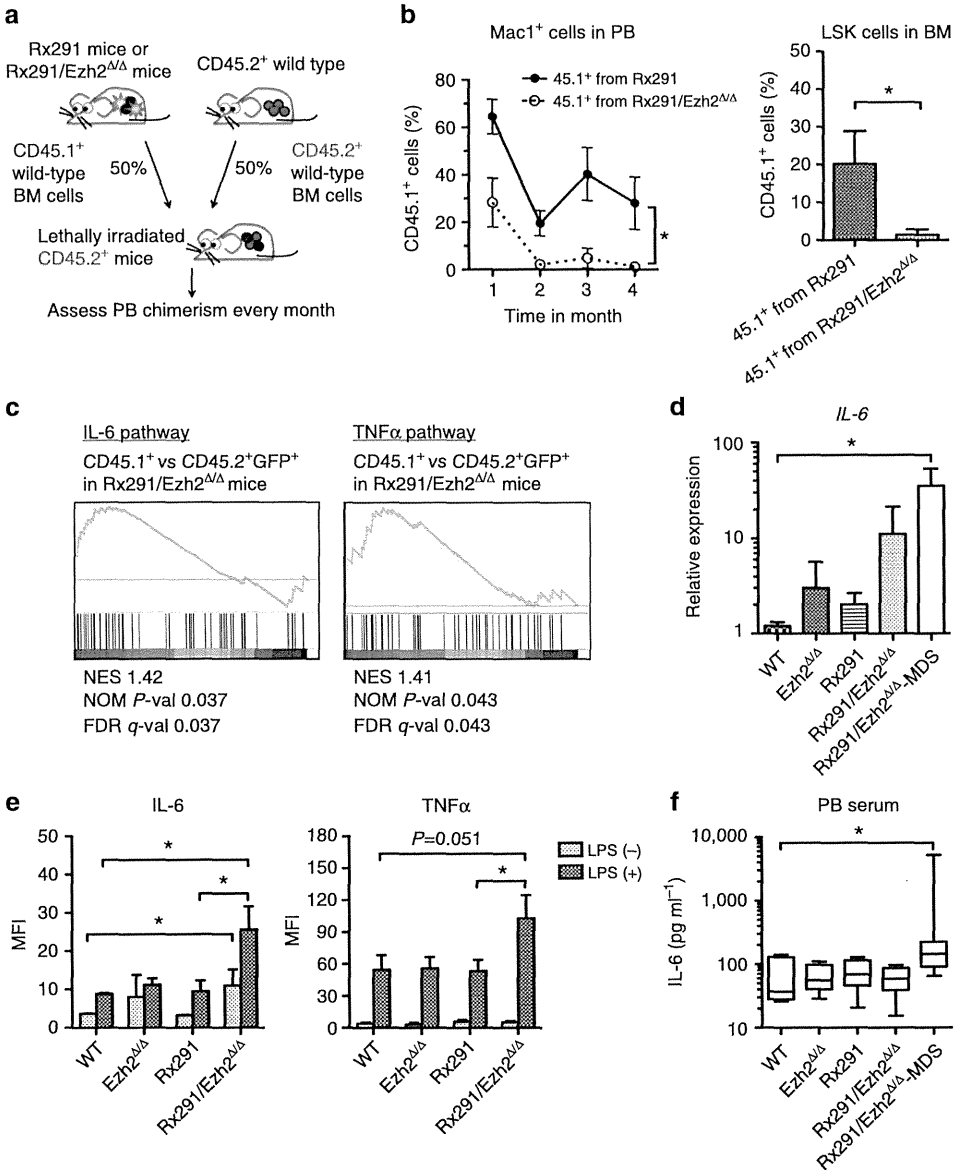

Figure 5 | Impaired normal HSPC functions in RUNX1S291fs/Ezh2-null mice. (**a**) Experimental scheme of analysing function of CD45.1$^+$ WT BM cells in Rx291 mice and Rx291/Ezh2$^{\Delta/\Delta}$ mice. CD45.1$^+$ WT (2×10^5) BM cells isolated from Rx291 and Rx291/Ezh2$^{\Delta/\Delta}$ mice were transplanted into lethally irradiated CD45.2$^+$ mice along with the same number of freshly isolated CD45.2$^+$ WT (2×10^5) BM cells. (**b**) Repopulation capacity of CD45.1$^+$ WT cells from Rx291 and Rx291/Ezh2$^{\Delta/\Delta}$ mice. Chimerism of CD45.1$^+$ Mac1$^+$ myeloid cells in PB (left panel) and LSK cells (right panel) in BM at 4 months post transplantation is depicted ($n=3$). Scale bars and asterisk show mean ± s.d. and *$P<0.05$ by Student's *t*-test. (**c**) Gene set enrichment plots for IL-6 (ref. 54) (left panel) and TNFα (TNF receptor signalling, Pathway Interaction Database)(right panel) pathway gene sets comparing CD45.1$^+$ WT LSK cells to CD45.2$^+$GFP$^+$ mutant LSK cells in Rx291/Ezh2$^{\Delta/\Delta}$ mice. (**d**) Quantitative RT-PCR analysis of the expression of *IL-6* in CD45.2$^+$GFP$^+$ LSK cells from WT, Ezh2$^{\Delta/\Delta}$, Rx291 and Rx291/Ezh2$^{\Delta/\Delta}$ mice at 4 months post transplantation (pre-MDS stage) and from moribund Rx291/Ezh2$^{\Delta/\Delta}$-MDS mice ($n=4$–5). Scale bars and asterisk show mean ± s.d. and *$P<0.05$ by Mann–Whitney *U*-test. (**e**) Levels of IL-6 and TNFα proteins in CD45.2$^+$GFP$^+$ BM cells from WT, Ezh2$^{\Delta/\Delta}$, Rx291 and Rx291/Ezh2$^{\Delta/\Delta}$ mice (at pre-MDS stage) ($n=3$–6) when cultured with or without 10 ng ml^{-1} LPS for 5 hours *in vitro*. Expression levels were examined by flow cytometry and shown in mean fluorescence intensity (MFI). Scale bars and asterisk show means ± s.e.m and *$P<0.05$ by Student's *t*-test. (**f**) Levels of IL-6 protein in the PB serum from WT, Ezh2$^{\Delta/\Delta}$, Rx291 and Rx291/Ezh2$^{\Delta/\Delta}$ mice (at pre-MDS stage) and from moribund Rx291/Ezh2$^{\Delta/\Delta}$-MDS mice ($n=6$–8). Expression levels were examined by enzyme-linked immunosorbent assay utilizing anti-IL-6 antibody and are shown as box and whisker plots, *$P<0.05$ by Mann–Whitney *U*-test.

infection[41,42]. GSEA revealed upregulation of genes related to interferon-γ and IL-6 pathways in CD45.1$^+$ WT LSK cells from Rx291/Ezh2$^{\Delta/\Delta}$ mice compared with WT LSK cells from WT mice (Supplementary Table 3), suggesting activation of inflammatory cytokine responses in residual normal HSPCs in Rx291/Ezh2$^{\Delta/\Delta}$ mice. Furthermore, upregulation of IL-6 and tumor necrosis factor alpha (TNFα) pathways was evident when we compared CD45.1$^+$ WT LSK cells with CD45.2$^+$-mutant LSK cells from the same Rx291/Ezh2$^{\Delta/\Delta}$ mice (Fig. 5c), but not from Rx291fs mice (Supplementary Fig. 6). Indeed, *Rx291/Ezh2$^{\Delta/\Delta}$*-MDS (CD45.2$^+$GFP$^+$) LSK cells significantly upregulated *IL-6*, compared with WT LSK cells (Fig. 5d). Given that IL-6 and TNFα impair normal HSC function *in vivo*[43], we examined levels of IL-6 and TNFα proteins in BM cells and circulating amount of IL-6 in PB serum. Levels of IL-6, but not TNFα, were significantly elevated in *Rx291/Ezh2$^{\Delta/\Delta}$* BM cells (Fig. 5e).

© 2014 Macmillan Publishers Limited. All rights reserved.